Hedging Cryptocurrency Options

Matic, Jovanka Lili and Packham, Natalie and Härdle, Wolfgang Karl

Humboldt-Universität zu Berlin, Hochschule für Wirtschaft und Recht Berlin, Humboldt-Universität zu Berlin

20 November 2021

Hedging Cryptocurrency Options[*]

Jovanka Matic[†]   Natalie Packham[‡]   Wolfgang Karl Härdle [§]

November, 2021

Abstract

The cryptocurrency (CC) market is volatile, non-stationary and non-continuous. This poses unique challenges for pricing and hedging CC options. We study the hedge behaviour and effectiveness for a wide range of models. First, we calibrate market data to SVI-implied volatility surfaces to price options. To cover a wide range of market dynamics, we generate price paths using two types of Monte Carlo simulations. In the first approach, price paths follow an SVCJ model (stochastic volatility with correlated jumps). The second approach simulates paths from a GARCH-filtered kernel density estimation. In these two markets, options are hedged with models from the class of affine jump diffusions and infinite activity Lévy processes. Including a wide range of market models allows to understand the trade-off in the hedge performance between complete, but overly parsimonious models, and more complex, but incomplete models. Dynamic Delta, Delta-Gamma, Delta-Vega and minimum variance hedge strategies are applied. The calibration results reveal a strong indication for stochastic volatility, low jump intensity and evidence of infinite activity. With the exception of short-dated options, a consistently good performance is achieved with Delta-Vega hedging in stochastic volatility models. Judging on the calibration and hedging results, the study provides evidence that stochastic volatility is the driving force in CC markets.

1 Introduction

Consider the problem of hedging contingent claims written on cryptocurrencies (CC). The dynamics of this new expanding market is characterized by high volatility, as is evident from the Cryptocurrency volatility index `VCRIX` (see Kim, Trimborn, and Härdle (2021)) and large price jumps (Scaillet, Treccani, and Trevisan, 2018). We approach hedging options written on `Bitcoin` (BTC) with models from the class of affine jump diffusion models and infinite activity Lévy processes. Similarly to Branger, Krautheim, Schlag, and Seeger (2012), we assess the hedge performance of implausible, yet complete as well as plausible, but incomplete asset pricing models. Since April 2019, contingent claims written on BTC and `Ethereum` (ETH) have been actively traded on `Deribit` (`www.deribit.com`). The Chicago Merchantile Exchange (CME) introduced options on BTC futures in January 2020. In contrast to traditional asset classes such as equity or fixed income, the market for CC options has only recently emerged and is still gaining liquidity, see e.g. (Härdle and Trimborn, 2015) for an early description of the market. Despite growing market volume, cryptocurrency markets continue to exhibit high volatility and frequent jumps, posing challenges to valuation and risk management. From the point of view of market makers and in the interest of financial stability, it is of high priority to understand and monitor risks associated with losses.

As the option market is still immature and illiquid, in the sense that quotes for many specific strikes or maturities are not directly observable or may be stale, we derive options prices by interpolating prices from stochastic volatility inspired (SVI) parametrized implied volatility (IV) surfaces (Gatheral, 2004). In order to capture a variety of market dynamics, the BTC market is imitated with two different Monte Carlo simulation approaches. In a parametric price path generation approach, we assume that the data-generating process is described by the SVCJ model. The second scenario generation method is based on GARCH-filtered Kernel-density estimation (GARCH-KDE) close to actual market dynamics. Under each of the two different market simulation methods, options are hedged where the hedger considers models of different complexity. This deliberately includes models that are "misspecified" in the sense that relevant risk factors may be omitted (Branger et al., 2012). On the other hand, those models are possibly parsimonious enough to yield a complete market. It is known that, when comparing the hedge performance to a more realistic, albeit incomplete market model, the simpler model may outperform the complex model (Detering and Packham, 2015). In our

context, a model is "misspecified" if it contains fewer or different parameters than the SVCJ model. Specifically, as models included in the class of SVCJ models, we consider the Black and Scholes (1973) (BS) model, the Merton (1976) jump-diffusion model (JD), the Heston (1993) stochastic volatility model (SV), the stochastic volatility with jumps model (SVJ) (Bates, 1996) and the SVCJ model itself. Infinite activity Lévy hedge models under consideration are the Variance-Gamma (VG) model (Madan, Carr, and Chang, 1998) and the CGMY model (Carr and Geman, 2002). Options are hedged dynamically with the following hedge strategies: Delta (Δ), Delta-Gamma ($\Delta - \Gamma$), Delta-Vega ($\Delta - \mathcal{V}$) and minimum variance strategies. To gain further insights, we separate the full time period, ranging from April 2019 to June 2020, into 3 different market scenarios with a bullish market behavior, calm circumstances with low volatility and a stressed scenario during the SARS-COV-2 crisis. In addition to evaluating the hedge performance, we aim to identify BTC risk-drivers such as jumps. This contributes to the understanding of what actually drives fluctuations on this market.

A number of papers investigate the still young market of CC options. Trimborn and Härdle (2018) describe the CC market dynamics via the cryptocurrency index `CRIX`. Madan, Reyners, and Schoutens (2019) price BTC options and calibrate parameters for a number of option pricing models, including the Black-Scholes, stochastic volatility and infinite activity models. Hou, Wang, Chen, and CYH (2020) price `CRIX` options under the assumption that the dynamics of the underlying are driven by the (SVCJ) model introduced in Duffie, Pan, and Singleton (2000) and Eraker, Johannes, and Polson (2003). To the best of our knowledge, hedging of CC options has not yet been investigated in this depth and detail. The aspect of risk management and the understanding of the dynamics of CCs is therefore a central contribution of this study.

The remainder of the paper is structured as follows: Section 2 describes the methodology, decomposed into market scenario generation, option valuation and hedge routine. The hedge routine presents the hedge models and explains the model parameter calibration and hedge strategy choices. In Section 3, we present and evaluate the results of the hedge routine and in Section 4, we conclude. The code is available as quantlets, accessible through `Quantlet` under the name **Q** hedging_cc.

behavior	$\hat{\mu}$	$\hat{\sigma}$	min	q_{25}	q_{50}	q_{75}	max
bullish	0.0038	0.0428	-0.1518	-0.0157	0.0050	0.0227	0.1600
calm	0.0009	0.0290	-0.0723	-0.0162	-0.0015	0.0098	0.1448
covid	0.0012	0.0490	-0.4647	-0.0107	0.0009	0.0162	0.1671

Table 2.1: Summary statistics of the bullish, calm and covid market log returns r_t ⚲hedging_cc

2 Methodology

In this section, we introduce the methodology, comprising market scenario generation, option valuation and hedging.

2.1 Market generation

We describe how to generate synthetic market data, which serves as the input for the remainder of the analysis. The principal goal of synthetic scenario generation is to imitate the BTC market behavior, especially retaining its statistical properties. Monte Carlo simulation provides the flexibility to create a large amount of plausible scenarios. In addition, we consider two simulation methods capturing different statistical properties. They represent a trade-off between a parametric model with valuable and traceable risk-factor information and a flexible non-parametric closer-to-actual-market approach. The parametric model is simulated under the risk neutral measure $\mathbb{Q}$ with a forward looking perspective. The non-parametric simulation relates to the past market behavior performed under the physical measure $\mathbb{P}$. The time frame under consideration is from 1st April 2019 to 30th June 2020. The BTC market behavior in this time period is time-varying. This makes it convenient to segregate the time frame into three disjoint market segments from April to September 2019 (*bullish*), October 2019 to February 2020 (*calm*) and March to June 2020 (*covid*), respectively. Bearing in mind that we are going to hedge 1-month and 3-month options, the minimal segment length is chosen to exceed three months. A graphical representation of the BTC closing price trajectory is illustrated in Figure 2.1 with the corresponding summary statistics in Table 2.1. The first interval is labeled as the *bullish* segment, because, to a great extent, the market behaves upward-trending. The second period labeled as the *calm period*. With an overall standard deviation $\hat{\sigma}$ = 756.55, price movements are more stagnant compared to the bullish segment. The last segment is the *Corona Crisis* or *stressed scenario*, where financial markets, especially

4
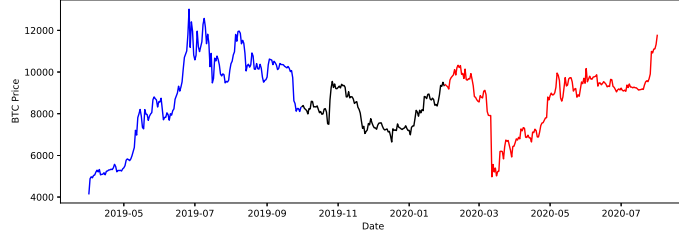
Figure 2.1: BTC closing price from 1st April 2019 to 30th June 2020, where the blue trajectory represents the bullish market behavior, the black path the calm period and red path the stressed scenario during the Corona Crisis.

🔍 LoadBTC

CC markets, experienced high volatility. A notable mention is the behavior of the BTC on 12th March 2020, where its price dropped by nearly 50%.

We now turn to a formal mathematical framework. Let the BTC market to be a continuous-time, frictionless financial market. Borrowing and short-selling are permitted. The constant risk-free interest rate $r \geq 0$ and the time horizon $T < \infty$ are fixed. On a filtered probability space $\left(\Omega, \mathcal{F}, (\mathcal{F}_t)_{t \in [0,T]}, \mathbb{P}\right)$, the asset price process and the risk-free asset are defined by adapted semimartingales $(S_t)_{t \geq 0}$ and $(B_t)_{t \geq 0}$, where $B_0 = 1$ and $B_t = e^{rt}$, $t \geq 0$, respectively. The filtration is assumed to satisfy the usual conditions (e.g. (Protter, 2005)). To ensure the absence of the arbitrage, we assume the existence of a risk-neutral measure $\mathbb{Q}$. We consider an option writer's perspective and short a European call option. The price of the option with strike K and time-to-maturity (TTM) $\tau = T - t$ at time $t < T$ is $C(t, \tau, K)$. For multiple-instrument hedges, we further assume the existence of a liquidly traded call option suitable for hedging $C_2(t, \tau, K_2)$, where $K_2 \neq K$. The dynamic hedging strategy $\xi = (\xi_0, \xi_1) = (\xi_0(t), \xi_1(t))_{0 \leq t \leq T}$ is an $\mathcal{F}$-predictable process, where $\xi_0(t)$ and $\xi_1(t)$ denote the amounts in the risk-free security and the asset, respectively. The resulting portfolio process $\Pi = (\Pi_t)_{t \geq 0}$ is admissible and self-financing. The evolution of the value process Π is reviewed in detail in Appendix .1, .2 and .3.

The finite time horizon T is partitioned into $T = \{0, \delta t, 2\delta t, \ldots, m\delta t = T\}$, where $m \in \mathbb{N}$ denotes the m-th trading day and $\delta t = \frac{1}{365}$. Scenarios are $N = 100000$ trajectories of the asset price process $S(t) = (S_{t,i})$, where $i = 1, \ldots, N$ and $t = 0, 1, \ldots T$. The parametric scenario generation approach assumes that the dynamics of the asset price process S_t and the volatility

process V_t are described by the SVCJ model introduced in Duffie et al. (2000). This particular choice is motivated by the methodology in Hou et al. (2020), where the model is applied to pricing options on the `CRIX`. A high degree of free parameters enables to model various market dynamics. Precisely, the model dynamics are

$$\frac{dS_t}{S_t} = \mu \delta t + \sqrt{V_t} dW_t^s + Z_t^s dN_t$$

$$dV_t = \kappa \left(\theta - V_t \right) \delta t + \sigma_v \sqrt{V_t} dW_t^v + Z_t^v dN_t \tag{1}$$

$$\text{Cov} \left\{ dW_t^s, dW_t^v \right\} = \rho \delta t$$

where W_t^s, W_t^v are two standard Wiener processes correlated with correlation coefficient ρ. The mean reversion speed is denoted by κ, θ is the mean reversion level and σ_v the scale of V_t. The model allows for contemporaneous arrivals of jumps in returns and jumps in volatility goverened by the Poisson process $N_t = N_t^s = N_t^v$ with constant intensity $\lambda = \lambda_s = \lambda_v$. Jump sizes in volatility Z_t^v are exponentially distributed $Z_t^v \sim \varepsilon \left(\mu_v \right)$ and jumps sizes in asset prices are conditionally normally distributed

$$\Xi \overset{def}{=} Z_t^s | Z_t^v \sim N \left(\overline{\mu}_s + \rho_j Z_t^v, \sigma_s^2 \right) \tag{2}$$

where $\overline{\mu}_s$ is the conditional mean jump size in the asset price given by

$$\overline{\mu}_s = \frac{\exp \left\{ \mu_s + \frac{(\sigma_s)^2}{2} \right\}}{1 - \rho_j \mu_v} - 1$$

In detail, μ_s is the unconditional mean, σ_s the jump size standard deviation and ρ_j is the correlation coefficient between jumps. From an empirical point of view, in most markets, jumps occur seldomly and are difficult to detect, and, as a consequence, the calibration of ρ_j is unreliable (Broadie, Chernov, and Johannes, 2007). We follow the recommendation of Broadie et al. (2007), Chernov, Gallant, Ghysels, and Tauchen (2003), Eraker et al. (2003), Eraker (2004) and Branger, Hansis, and Schlag (2009) and set $\rho_j = 0$. Furthermore, the risk premium is set to zero, so that $\mu = r$ and $\mathbb{P} = \mathbb{Q}$. The resulting paths are simulated according to the Euler-Maruyama discretization of (1) suggested in Belaygorod (2005). The corresponding model parameters are re-calibrated daily according to the methodology described in section 2.3.2.

Compared to the empirical price process, the SVCJ may appear quite restrictive: aside from being an incomplete market model, the price dynamics are limited by the specification of

the stochastic volatility component as well as the jump intensity and size. The nonparametric method loosens the assumptions by generating scenarios using GARCH-filtered kernel density estimation (GARCH-KDE) as in e.g. McNeil and Frey (2000). Let (r_t) denote BTC log-returns and $(\hat{\sigma}_t)$ the estimated GARCH(1,1) volatility (Bollerslev, 1986). The kernel density estimation is performed on "de-garched" residuals

$$\hat{z}_t = \frac{r_t}{\hat{\sigma}_t}. \tag{3}$$

The rationale is to capture the time-variation of volatility by the GARCH filter and perform kernel density estimation on standardised residuals. The estimated density function is

$$\widehat{f_h}(z) = \frac{1}{nh} \sum_{t=1}^{n} K\left(\frac{\hat{z}_t - z}{h}\right), \tag{4}$$

where K denotes the Gaussian Kernel. The resulting generated paths are

$$S(T) = S(0) \exp\left[\sum_{t=1}^{T} \hat{\sigma}_t \hat{z}_t\right] \tag{5}$$

Throughout this paper, the parametric and the nonparametric method are referred to as the SVCJ and GARCH-KDE framework, respectively.

2.2 Valuation

This section describes how option prices are derived from the market IV quotes. As the market for CC claims, during the time period of our dataset, is still relatively immature with only a limited number of actively traded options on `Deribit` and the Chicago Mercantile Exchange, arbitrage-free option prices are derived through the stochastic volatility inspired (SVI) parameterization of the volatility surface of Gatheral and Jacquier (2014). Let $\sigma_{\mathrm{BS}}(k,\tau)$ denote the BS IV with log-moneyness $k = \log(K/S_0)$ and total implied variance $w(k,\tau) = \sigma_{\mathrm{BS}}^2(k,\tau)\tau$. For a fixed τ, the raw SVI parameterization of a total implied variance smile as initially presented in Gatheral (2004) is

$$w\left(k; \chi_R\right) = a + b\left\{\rho(k-m) + \sqrt{(k-m)^2 + \sigma^2}\right\}. \tag{6}$$

In the parameter set $\chi_R = \{a, b, \rho, m, \sigma\}$, $a \in \mathbb{R}$ governs the general level of variance, $b \geq 0$ regulates the slopes of the wings, $\rho \in [-1, 1]$ controls the skew, $m \in \mathbb{R}$ enables horizontal smile shifts and $\sigma > 0$ is the ATM curvature of the smile (Gatheral and Jacquier, 2014). For each maturity, the smile is recalibrated daily. The implied volatility is obtained by a

simple root-finding procedure, whereas the parameters χ_R are calibrated according to the optimization technique explained in Section 2.3.2. In addition, the calibration is subject to non-linear constraints prescribed in Gatheral and Jacquier (2014). These constraints ensure convexity of the option price which rules out butterfly arbitrage. Calendar spread arbitrage is avoided by penalizing fitted smiles which induce a decrease in the level of the total implied variance for a given strike level. For interpolation, the ATM total implied variance $\theta_T = w(0, T)$ is interpolated for $t_1 < T < t_2$ as in Gatheral and Jacquier (2014). The resulting option price $C(T, K)$ is a convex combination

$$\alpha_T = \frac{\sqrt{\theta_{t_2}} - \sqrt{\theta_T}}{\sqrt{\theta_{t_2}} - \sqrt{\theta_{t_1}}} \in [0, 1]$$

$$C(T, K) = \alpha_T C(t_1, K) + (1 - \alpha_T) C(t_2, K).$$

(7)

2.3 Hedge routine

This section describes the models selected to hedge BTC options as well as the model parameter calibration procedure. Given these model classes, hedge strategies are chosen for the hedge routine.

2.3.1 Hedge models

For hedging purposes, the choice of a hedge model faces the trade-off between sufficient complexity to describe the actual market dynamics and market completeness (Detering and Packham, 2015). In practice, a trader may therefore initiate hedging with an evidently wrong but simple model, such as the complete BS option pricing model. A lower number of parameters provides a parsimonious setup with potentially manageable explanatory power. In our setting, a European option is hedged employing models of increasing complexity. In the following, the model granularity is gradually extended by the addition of risk-factors such as local volatility, jumps, stochastic volatility and others. This covers the empirical finding of the previous literature on CC's, e.g. (Kim et al., 2021; Scaillet et al., 2018). Accordingly, the hedge models selected encompass affine jump diffusion models and infinite activity Levy processes.

The class of affine jump diffusion models covers well-known models nested in (1). Due to its popularity in the financial world, the simple but complete BS option pricing is selected as

a hedge model. The volatility is constant with $V_t = \sigma$ and there are no discontinuities from jumps $N_t^s = N_t^v = 0$. A slightly more complex model is the JD model. It assumes constant volatility with $V_t = \theta$, $\sigma_V = 0$ and extends the BS model by allowing for jumps in returns, but with $N_t^v = 0$. The jump size is $\log \xi \sim N\left(\mu_s, \delta_s^2\right)$ distributed.

Evidence for stochastic volatility motivates the choice of the SV model. The jump component is excluded with $\lambda = 0$ and $N_t^s = N_t^v = 0$. We also examine the SVCJ model itself as a model used for hedging. It serves as the most general model and its hedge performance provides a meaningful insight for the comparison of the SVCJ and GARCH-KDE framework, while in the SVCJ framework, it provides "anticipated" hedge results (cf. Branger et al. (2012)). Due to the jump scarcity and latent nature of the variance process V_t, we also consider the SVJ model for hedging. In this model, the jump component in the variance process V_t is dropped while keeping the jump component in the spot process S_t, i.e. $N_t^v = 0$.

In contrast to affine jump processes, there exists a well-established class of processes that do not entail a continuous martingale component. Instead, the dynamics are captured by a right-continuous pure jump process, such as the Variance Gamma (VG) model (Madan et al., 1998). The underlying S_t evolves as

$$
\begin{aligned}
dS_t &= rS_{t-}dt + S_{t-}dX_t^{\mathrm{VG}} \\
X_t^{\mathrm{VG}} &= \theta G_t + \sigma W_{G_t},
\end{aligned}
\tag{8}
$$

with the characteristic function of the VG-process X_t^{VG} given by

$$
\varphi_{\mathrm{VG}}(u; \sigma, \nu, \theta) = \left(1 - \mathrm{i}u\theta\nu + \frac{1}{2}\sigma^2\nu u^2\right)^{-1/\nu},
\tag{9}
$$

where r is the risk-free rate, W_t is a Wiener process and G_t is a Gamma process. The overall volatility level is represented by σ; θ governs the symmetry of the distribution and therefore controls the implied volatility skew; ν controls for tails, kurtosis and thus regulates the shape of the volatility surface. An alternative representation of the VG process pleasant for practical interpretation has the characteristic function

$$
\varphi_{\mathrm{VG}}(u; C, G, M) = \left(\frac{GM}{GM + (M - G)\mathrm{i}u + u^2}\right)^C,
\tag{10}
$$

where C, G, $M > 0$. The detailed link between (9) and (10) is described in Appendix .4. An increase in G (M) increases the size of upward jumps (downward jumps). Accordingly, θ, M and G account for the skewness of the distribution. An increase in C widens the Levy-measure.

An extension of the VG model is the CGMY model by Carr and Geman (2002). On a finite time interval, the additional parameter Y permits infinite variation as well as finite or infinite activity. Formally, in (8) the source of randomness is replaced by a CGMY process X_t^{CGMY} with the characteristic function

$$\varphi_{\mathrm{CGMY}}(u; C, G, M, Y) = \exp\left[Ct\Gamma(-Y)\left\{(M - \mathrm{i}u)^Y - M^Y + (G + \mathrm{i}u)^Y - G^Y\right\}\right]. \qquad (11)$$

The X_t^{VG}-process in the representation in equation (9) is a special case of the CGMY process for $Y = 1$. On a finite time interval, the behavior of the path depends on Y. For $Y < 0$, there is a finite number of jumps, else infinite activity. In case of $Y \in (1, 2]$, there is also infinite variation.

2.3.2 Calibration routine

The model parameters are calibrated following to the FFT option pricing technique of Carr and Madan (2001). The price of a European-style option $C(K, T)$ is given by

$$
\begin{aligned}
C(K, T) &= \frac{1}{\pi} \mathrm{e}^{-\alpha \log(K)} \int_0^\infty \mathrm{e}^{-\mathrm{i}v \log(K)} \rho(v) dv \\
\rho(v) &= \frac{\varphi_T(v - (\alpha + 1)\mathrm{i})}{\alpha^2 + \alpha - v^2 + \mathrm{i}(2\alpha + 1)v},
\end{aligned}
\qquad (12)
$$

where $c_T(k)$ denotes the α-damped option price $c_T(k) = e^{\alpha k} C_T(k)$ and $\varphi_{c_T}(t)$ its characteristic function. The ill-posed nature of calibration can lead to extreme values of the model parameters. This is avoided by employing a Tikhonov L_2-regularization (Tikhonov, Leonov, and Yagola, 2011). At the cost of accepting some bias, this penalizes unrealistic values of the model parameters by giving preference to parameters with smaller norms.

Calibration is performed by the optimizer

$$
\begin{aligned}
\theta^* &= \underset{\theta \in \Theta}{\operatorname{argmin}} R(\theta) \\
R(\theta) &= \sqrt{\frac{1}{n} \sum_i \{IV_{Model}(h_i, \theta) - IV_{Market}((T_i, K_i))\}^2} + \theta^\top \Gamma \theta,
\end{aligned}
\qquad (13)
$$

where Γ is a diagonal positive semi-definite matrix. The matrix Γ corresponds to the Tikhonov L_2-regularization, which gives preference to parameters with smaller norms. The entries in the matrix Γ are chosen individually for each parameter to ensure that they maintain the same reasonable order of magnitude.

The parameter space $\Theta \subset \mathbb{R}^d$ of each model in scope is subject to linear inequality constraints. Given that the objective is not necessarily convex, it may have multiple local minima. In order to explore the entire parameter space, simplex-based algorithms are more appropriate than local gradient-based techniques. In our case, we employ the Sequential Least Squares Programming optimization (Kraft, 1988) routine. We adjust for time effects by calibrating parameters on the IV surface instead of option prices. As deep out-of-the-money or deep in-the-money instruments do not provide valuable input for calibration in our case, the Δ_{25} criterion is imposed: all claims whose Δ_{BS} is smaller than 0.25 or larger than 0.75 in terms of the absolute value, that is $0.25 < |\Delta_{Market}| < 0.75$, are disregarded.

2.3.3 Hedging strategies

To protect against broad market movements, we examine hedging with market-risk-related sensitivities $(\Delta, \Gamma, \mathcal{V}) = \left(\frac{\partial C}{\partial S}, \frac{\partial^2 C}{\partial^2 S}, \frac{\partial C}{\partial \sigma} \right)$. The goal is to protect the position against first-order changes in the underlying $S = \{S_t, \ t \in T\}$, second-order changes (i.e., first-order changes in Δ) and to changes in σ, respectively. To achieve $\Delta - \Gamma$- or $\Delta - \mathcal{V}$-neutrality, an additional liquid option $C_2(S(t), T, K_1)$ with strike $K_1 \neq K$ is priced from the **SVI** parameterized **IV** surface, as explained in Section 2.2. For performance comparison of linear and non-linear effects, the dynamic Δ- and $\Delta - \Gamma$-hedging strategies are applied to all hedge models. The $\Delta - \mathcal{V}$-hedge is only considered for affine jump diffusion models, since $\mathcal{V}$ is not a risk-factor of the infinite activity Lévy-processes under consideration. The technical aspects of the dynamic hedging strategies are described in Appendices .2 and .3. Models that incorporate jumps are incomplete and difficult to hedge. Jumps and infinite activity Lévy processes are therefore often hedged with quadratic variance-related hedging strategies. Under the assumption of symmetric losses and gains, the aim is to find the strategy ξ^* under $\mathbb{Q}$ that minimizes the hedging error in terms of the mean-squared error (Föllmer and Sondermann, 1985)

$$(\Pi(0), \xi^*(t)) = \operatorname*{argmin}_{\Pi(0), \xi_1(t)} \mathsf{E}_{\mathbb{Q}} \left[\left(C_T - \Pi(0) - \int_0^T \xi_1(u) dS(u) \right)^2 \right]. \tag{14}$$

Table 2.2 summarizes the hedging strategies applied to the respective hedge models. The calibrated model parameters are used to compute hedging strategies $\xi(t)$ for each model.

Each model's hedge performance is evaluated by indicators derived from the relative Profit-and-Loss (PnL)

$$\pi_{\mathrm{rel}} = e^{-rT} \frac{\Pi_T}{C\{S_0, K, T\}}. \tag{15}$$

model	tailored hedge	strategy comparison
Black-Scholes	Δ_{BS}	$\Delta - \Gamma_{BS}$, $\Delta - \mathcal{V}_{BS}$
SV	$\Delta - \mathcal{V}_{Heston}$	**MV**, Δ_{Heston}, $\Delta - \Gamma_{Heston}$
JD	**MV**	Δ_{JD}, $\Delta - \Gamma_{JD}$, $\Delta - \mathcal{V}_{JD}$
SVJ	**MV**	Δ_{SVJ}, $\Delta - \Gamma_{SVJ}$, $\Delta - \mathcal{V}_{SVJ}$
SVCJ	**MV**	Δ_{SVCJ}, $\Delta - \Gamma_{SVCJ}$, $\Delta - \mathcal{V}_{SVCJ}$
VG	**MV**	Δ_{VG}, $\Delta - \Gamma_{VG}$
CGMY	**MV**	Δ_{CGMY}, $\Delta - \Gamma_{VG}$

Table 2.2: Hedge strategy summary, where a *tailored hedge* refers to the proposed hedge model and *strategy comparison* refers other hedges applied for comparison.

In a perfect hedge in a complete market we have $\pi_{rel} = 0$. However, in practice, due to model incompleteness, discretization and model uncertainty, $\pi_{rel} \neq 0$. We evaluate the hedge performance with the relative hedge error ε_{hedge} as applied in e.g. Poulsen, Schenk-Hoppé, and Ewald (2009), defined as

$$\varepsilon_{hedge} = 100\sqrt{\text{Var}\left(\pi_{\text{rel}}\right)}. \tag{16}$$

The rationale behind ε_{hedge} is that standard deviation represents a measure of uncertainty. A sophisticated hedge strategy reduces or ideally eliminate uncertainty (Branger et al., 2012). The tail behavior is evaluated by the expected shortfall

$$\text{ES}_\alpha = \mathbb{E}\left[\pi_{rel} \mid \pi_{rel} > F^{-1}_{\pi_{rel}}(\alpha)\right]. \tag{17}$$

3 Empirical results

3.1 Data

Models are calibrated on the market prices of European-style `Deribit` options written on BTC futures. Quotes and BTC prices are provided by `Tardis.dev` and the Blockchain Research Center `BRC`. The number of liquidly traded instruments varies significantly with maturity. Therefore, the data is filtered with liquidity cut-offs. All claims without trading volume are disregarded. In addition, the Δ_{25}-criterion is imposed.

|	F_0	1 M	3 M
BULLISH	4088.16	206.38	417.87
CALM	8367.51	838.01	1449.82
COVID	9804.85	610.36	1201.46

Table 3.1: Interpolated option prices for initial underlying price $F(0)$ and strike K_{ATM} for maturities $T = \{1\ \text{M}, 3\ \text{M}\}$. **Q**hedging_cc

period	mean	std	skew	kurt	q_{25}	q_{50}	q_{75}
BULLISH	0.13	0.99	0.17	0.87	-0.44	0.15	0.66
CALM	-0.02	0.74	0.34	0.12	-0.51	-0.06	0.38
COVID	0.05	0.70	-0.04	0.23	-0.34	0.04	0.47

Table 3.2: Summary statistics of estimated historical densities $\hat{z}_t$ defined in (3) for a respective scenario. **Q**hedging_cc

3.2 Option pricing

Option prices are obtained at every day of the hedging period. This is necessary for the calculation of the initial value of the hedging portfolio and to perform multi-asset dynamic hedging. Each option is priced according to the IV surface on the given day. If the option is not traded for the given strike or maturity, the SVI parametrized IV surface is interpolated in an arbitrage-free way. For illustration, we take a look at CC option prices at the beginning of each market period. Figure 3.1 displays the SVI parametrized interpolated IV surfaces for SVI parameters listed in Table .1. The resulting option prices used in the hedging routine are displayed in Table 3.1. Recall that for a given IV surface the SVI parameters related by the formula (6) are calibrated for each TTM. The temporal dynamics of the SVI parameters provide the following insights: parameter **a** increases with TTM, which aligns with the increase of the ATM total variance as TTM rises. Parameter σ decreases with TTM, indicating decrease of the ATM curvature. Increasing values of parameter **b** indicate higher slopes of the wings as TTM increases. Skewness, expressed in terms of the parameter ρ, varies across market segments. Usually negative values of ρ indicate a preference for OTM puts over OTM calls. In the bullish period, skewness is close to zero across most maturities.

(a) bullish   **(b)** calm   **(c)** covid
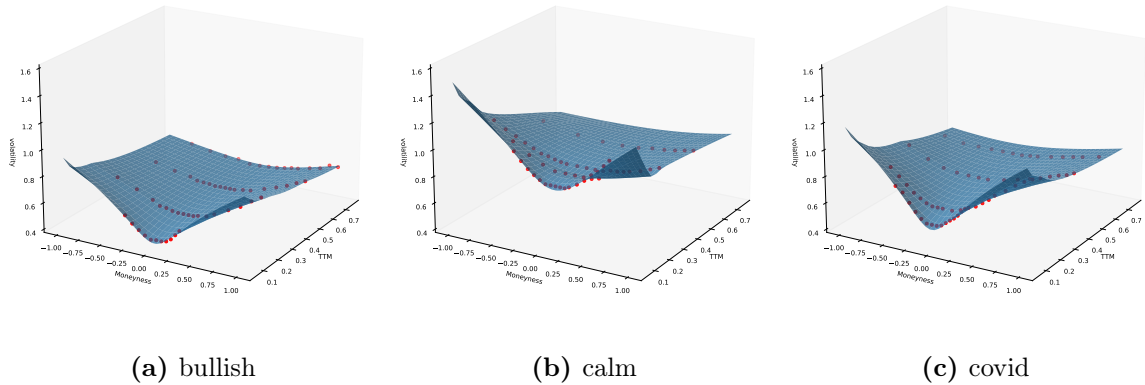
Figure 3.1: Market IVs in red and interpolated IV surface in blue on (a) 1st April 2019 (b) 1st October 2019 (c) 1st February 2020. Fitted smiles with very short maturities of $\tau \leq 1$ week are excluded from plots, because they are not relevant for the hedging routine. Calibrated SVI parameters shorter maturities are given in Table .1. **Q** hedging_cc

3.3 Scenario generation results

For the GARCH-KDE approach, the estimated residual distributions $\widehat{f}_h(z)$ from (4) are displayed in Figure 3.2. The empirical moments and quantiles are listed in Table 3.2. Figure .1 illustrates the GARCH(1, 1) estimates of BTC returns. As a consequence from *de-garching*, all three distributions are roughly symmetric and mean-zero. Deviations are direct results from market moves: the upward-moving market behavior in the *bullish* period leads to a left-skewed residual distribution. High drops in the *stressed* period result in a negatively skewed distribution.

SVCJ paths are simulated with daily re-calibrated parameters, which are summarized in Table 3.5. Selected statistical properties of both scenario generation approaches are given in Table 3.3. We observe differences in tails, extreme values and standard deviation. Discrepancies in $\hat{\sigma}$ are natural consequences from different methodological assumptions. The SVCJ approach assumes volatility to be stochastic, whereas GARCH-KDE models σ_t with GARCH(1,1). Discrepancies in path extremes result from the SVCJ model assumptions on return jump size Ξ_{SVCJ} in (2). In the calibration routine, the L_2-regularization is applied to control extreme parameter values. Yet, estimated return jump sizes can be very large. Resulting Euler discretized paths contain trajectories with extreme moves of the underlying. These are

14
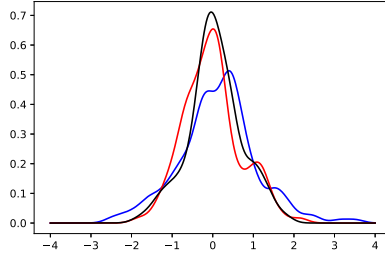
Figure 3.2: Estimated residual density $\widehat{f_h}(z)$ in (4) during bullish market behavior, calm period and the stressed scenario during the Corona Crisis for $h = 0.2$ 🔍hedging_cc

framework	$\hat{\mu}$	$\hat{\sigma}$	min	q_1	q_{50}	q_{99}	max
$SVCJ_{\text{BULLISH}_{30}}$	4087.32	343.05	1352.90	3411.83	4065.04	5177.02	15819.48
$SVCJ_{\text{CALM}_{30}}$	8369.33	1650.21	646.68	3475.29	8367.51	13092.95	26271.20
$SVCJ_{\text{COVID}_{30}}$	9800.32	1269.66	1435.49	5406.93	9804.85	13341.72	41464.61
$KDE_{BULLISH_{30}}$	4393.95	606.01	2089.55	3237.62	4277.65	6248.48	10209.30
$KDE_{\text{CALM}_{30}}$	8359.21	746.38	4545.46	6608.25	8349.06	10524.45	15611.32
$KDE_{\text{COVID}_{30}}$	9933.81	836.48	5579.96	8007.32	9848.62	12365.51	16863.17
$SVCJ_{\text{BULLISH}_{90}}$	4087.50	657.29	419.77	2961.11	4001.56	6336.31	56189.20
$SVCJ_{\text{CALM}_{90}}$	8367.54	2982.34	37.40	2488.41	8124.74	18415.20	118249.15
$SVCJ_{\text{COVID}_{90}}$	9796.71	2456.05	119.85	3620.50	9682.93	17545.53	115020.35
$KDE_{BULLISH_{90}}$	5116.43	1419.86	1325.30	3038.41	4762.11	9988.82	28593.53
$KDE_{\text{CALM}_{90}}$	8345.58	1407.72	3034.41	5341.07	8274.30	12590.88	22406.78
$KDE_{\text{COVID}_{90}}$	10718.15	3457.73	1560.16	4729.19	10007.73	23519.87	81081.55

Table 3.3: Summary statistics of scenario generations framework per market segment and maturity 🔍hedging_cc

e.g. extremely low and high prices during the calm and stressed scenario displayed in Table 3.3. The sometimes erratic BTC price evolution suggests that such price moves are entirely implausible.

3.4 Calibration results

In each period, calibration is performed daily using instruments satisfying the Δ_{25}-criterion. For an overview, average numbers of options per maturity range used for calibration are summarized in Table 3.6. As a consequence of the Δ_{25}-criterion, more longer-dated options are selected. The average parameter values per period are summarized in Table 3.5. Section 3.4.1 and 3.4.2 provide a detailed perspective on the dynamics of the calibrated parameters.

segment	$\hat{\mu}$	$\hat{\sigma}$	min	q_1	q_{50}	q_{99}	max
bullish	-0.03	0.18	-0.39	-0.37	-0.00	0.46	0.61
calm	-0.23	0.24	-0.44	-0.43	-0.34	0.53	0.58
covid	-0.28	0.17	-0.49	-0.48	-0.33	0.11	0.67

Table 3.4: Summary statistics of calibrated SVCJ jump size Ξ per market segment. ⚲hedging_cc

period	κ	ρ	V_0	θ	σ	λ	μ_y	σ_y	μ_v
$BS_{bullish}$	-	-	-	-	0.84	-	-	-	-
BS_{calm}	-	-	-	-	0.68	-	-	-	-
BS_{covid}	-	-	-	-	0.78	-	-	-	-
$Merton_{bullish}$	-	-	-	-	0.17	0.11	0.0	0.82	-
$Merton_{calm}$	-	-	-	-	0.42	0.72	0.0	0.55	-
$Merton_{covid}$	-	-	-	-	0.48	0.40	0.0	0.69	-
$SV_{bullish}$	0.75	0.16	0.76	0.42	0.82	-	-	-	-
SV_{calm}	1.60	0.17	0.35	1.10	0.68	-	-	-	-
SV_{covid}	1.43	0.01	0.63	0.95	0.56	-	-	-	-
$SVJ_{bullish}$	0.72	0.15	0.75	0.42	0.80	0.16	0.01	0.0	-
SVJ_{calm}	1.28	0.18	0.33	1.05	0.68	0.37	0.01	0.0	-
SVJ_{covid}	0.98	0.14	0.50	0.74	0.72	0.86	-0.15	0.0	-
$SVCJ_{bullish}$	0.51	0.14	0.74	0.09	0.88	0.31	-0.04	0.0	0.45
$SVCJ_{calm}$	0.75	0.28	0.30	0.38	0.83	0.85	-0.30	0.0	0.99
$SVCJ_{covid}$	0.61	0.22	0.52	0.18	0.89	1.04	-0.35	0.0	0.54

Table 3.5: Average calibrated parameters of affine jump diffusion models per market segment. ⚲hedging_cc

Calibration is carried out on the market's mid IVs. Of course, ignoring bid-ask spreads and the possibility of stale prices may produce arbitrage opportunities as well as spikes in parameters and calibration errors. However, this is considered a minor issue and ignored. RMSE's for the models are illustrated in Appendix .7. Naturally, the model fit improves with increasing model complexity. Hence, the BS model has the highest RMSE values on average while the SVCJ model has the lowest.

3.4.1 Affine jump diffusion models

The calibrated parameter σ_{BS} provides meaningful insights into market expectations. Levels vary in the range $\sigma_{BS} \in [50\ \%, 175\ \%]$, with summary statistics for this parameter provided in Table 3.7. Due to the volatile nature of the CC markets, levels of σ_{BS} are generally higher than in traditional markets (Madan et al., 2019). In comparison, the VIX index in the

period / maturity	≤ 1 W	(1 W, 2 W]	(2 W, 3 M]	(3 M, 6 M]	(6 M, 9 M]
bullish	2.77	1.72	4.61	7.14	2.53
calm	2.53	2.24	3.75	4.28	3.18
crisis	3.00	3.03	4.44	5.58	5.33

Table 3.6: Overview of average maturity counts of all options in a daily **IV** surface fullfiling the Δ_{25}-selection criteria. 🔍hedging_cc

behavior	average σ_{BS}	std. dev.	min	q_{25}	q_{50}	q_{75}	max
bullish	0.84	0.16	0.50	0.72	0.85	0.97	1.20
calm	0.68	0.06	0.61	0.64	0.66	0.70	0.89
stressed	0.78	0.21	0.57	0.63	0.73	0.87	1.75

**Table 3.7:** Summary statistics of daily σ_{BS} calibration.🔍hedging_cc

time period 1990-2021 ranges between 9.5% and 60%, with the 95%-quantile at 33.5%. Figure 3.3 shows the dynamics of σ_{BS} over the entire time frame. In the bullish period, volatility levels rise up to 120%. In the calm period, as expected, the levels are lower than in the other two periods with $\sigma_{BS} \in [0.61, 0.91]$. Figure 3.4 plots the calibrated parameters σ_{JD} and λ_{JD}
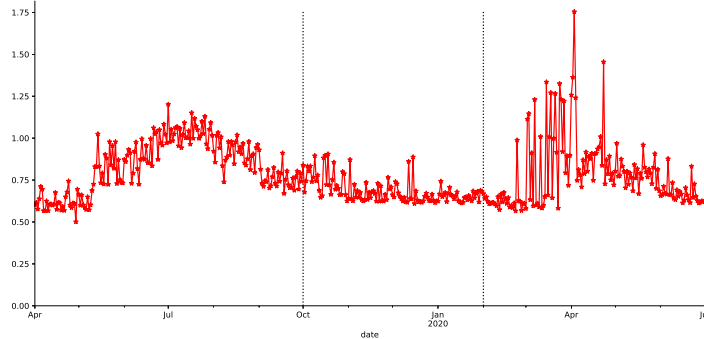
Figure 3.3: Daily calibration σ_{BS} segregated by market segment in chronological order. Volatility levels are very high compared to equities or indices such as S & P 500 🔍hedging_cc

of the JD model over time. In general, levels of σ_{JD} are lower than σ_{BS}, clearly visible during the *calm* and *stressed* scenario. As the JD model is an extension of the BS model, higher levels of σ_{BS} are partially compensated by the jump component. On many days σ_{JD} is close to σ_{BS}. The reason for this are generally low values of the annual jump intensity λ_{JD} and

jump size μ_y. On average, the JD model expects less than one jump in returns per year. The
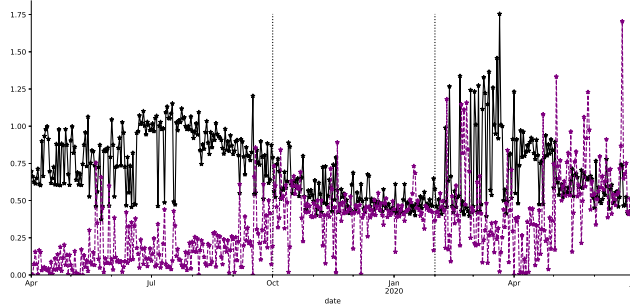
Figure 3.4: Interplay between σ_{JD} and λ_{JD} segregated by market segment in chronological order. Mostly, for high levels of σ_{JD} we observe low levels of λ_{JD} and vice versa. 🔍hedging_cc

evolution of λ_{JD} is compared to the jump intensities of extended models λ_{SVJ} and λ_{SVCJ} in Figure Appendix .2. Throughout, yearly jump intensities are low with mostly $\lambda_{SV(C)J} \leq 2.5$. We observe contrasting levels of λ_{SVCJ} and λ_{JD}. They are not directly comparable, as the jump intensity λ_{SVCJ} contributes to simultaneous jumps in returns and stochastic volatility, while λ_{JD} and λ_{SVJ} corresponds solely to jumps in returns. For example, levels of λ_{SVCJ} in the calm period are high whereas λ_{SVJ} is close to zero.

The plausibility of the stochastic volatility assumption is analyzed by the evolution and levels of σ_v. In most periods, levels of σ_v are higher compared to traditional markets. In the broad picture, the evolution of σ_v does not depend on model choice a shown in Figure Appendix .3. Table .2 summarizes statistical properties of this parameter by model and market segment. In the *bullish* and *calm* period, the indication for stochastic volatility is strong with vol-of-vol levels at $q_{50} \geq 80\%$ and $q_{50} \geq 75\%$, respectively. In the *stressed* period, levels of $\sigma_{v_{SV(C)J}}$ remain high for $q_{50} \geq 73\%$.

Empirical evidence suggests that in traditional markets the correlation parameter $\rho_{SV(CJ)}$ is usually negative. Specifically, when prices fall, volatility increases. However, across all three market segments and models, $\rho_{SV(CJ)}$ is mainly positive and close to zero as illustrated in Figure Appendix .4. Hou et al. (2020) name this phenomenon the *inverse leverage effect* in CC markets. This relationship in the CC markets is also supported by the correlation between the CRIX and the VCRIX under the physical measure $\mathbb{P}$. Pearson's correlation coefficient is

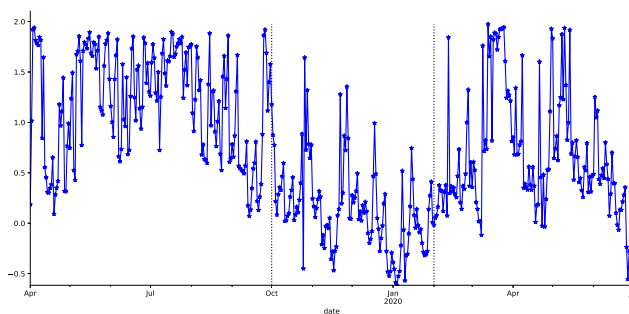| market segment	C	G	M	Y
$CGMY_{bullish}$	4.24	22.21	24.79	1.20
$CGMY_{calm}$	10.37	7.67	9.30	0.14
$CGMY_{covid}$	7.94	11.38	17.24	0.68

Table 3.8: Average calibrated parameters of the CGMY model segregated by market segment.

$\rho_{pearson}$ = 0.51 in the *bullish* and $\rho_{pearson}$ = 0.64 in the *calm* period, respectively. In the stressed segment, correlation is negative with $\rho_{pearson}$ = −0.73.

3.4.2 VG and CGMY

The prospect of infinite variation is evaluated by the calibration of the CGMY model with average calibrated parameters in Table 3.8. Precisely, we are interested in the evolution of the infinite activity parameter Y_{CGMY} portrayed in Figure 3.5. In each market segment, as $Y > 0$ widely, there is strong evidence for infinite activity. In the bullish period, for $Y_{CGMY} \in (1, 2]$ largely, there is also evidence for infinite variation (Carr and Geman, 2002). The bullish period catches high magnitudes of jump size direction increase parameters

Figure 3.5: Daily calibration of Y_{CGMY} segregated by market segment. As $Y_{CGMY} > 0$, there is strong indication for infinite activity. For $Y_{CGMY} \in (1, 2]$ in the bullish segment, there is evidence for infinite variation. **Q**hedging_cc

G_{CGMY} and M_{CGMY}, reflecting the nature of this market segment. Similarly, the increase in decreased jump size parameter M_{CGMY} is mainly higher in the stressed scenario. A graphical illustration is given in Figure Appendix .6. The **VG** is calibrated under representation (9). Overall, volatility levels of σ_{VG} are comparable to σ_{BS}, as illustrated in Figure Appendix .5.
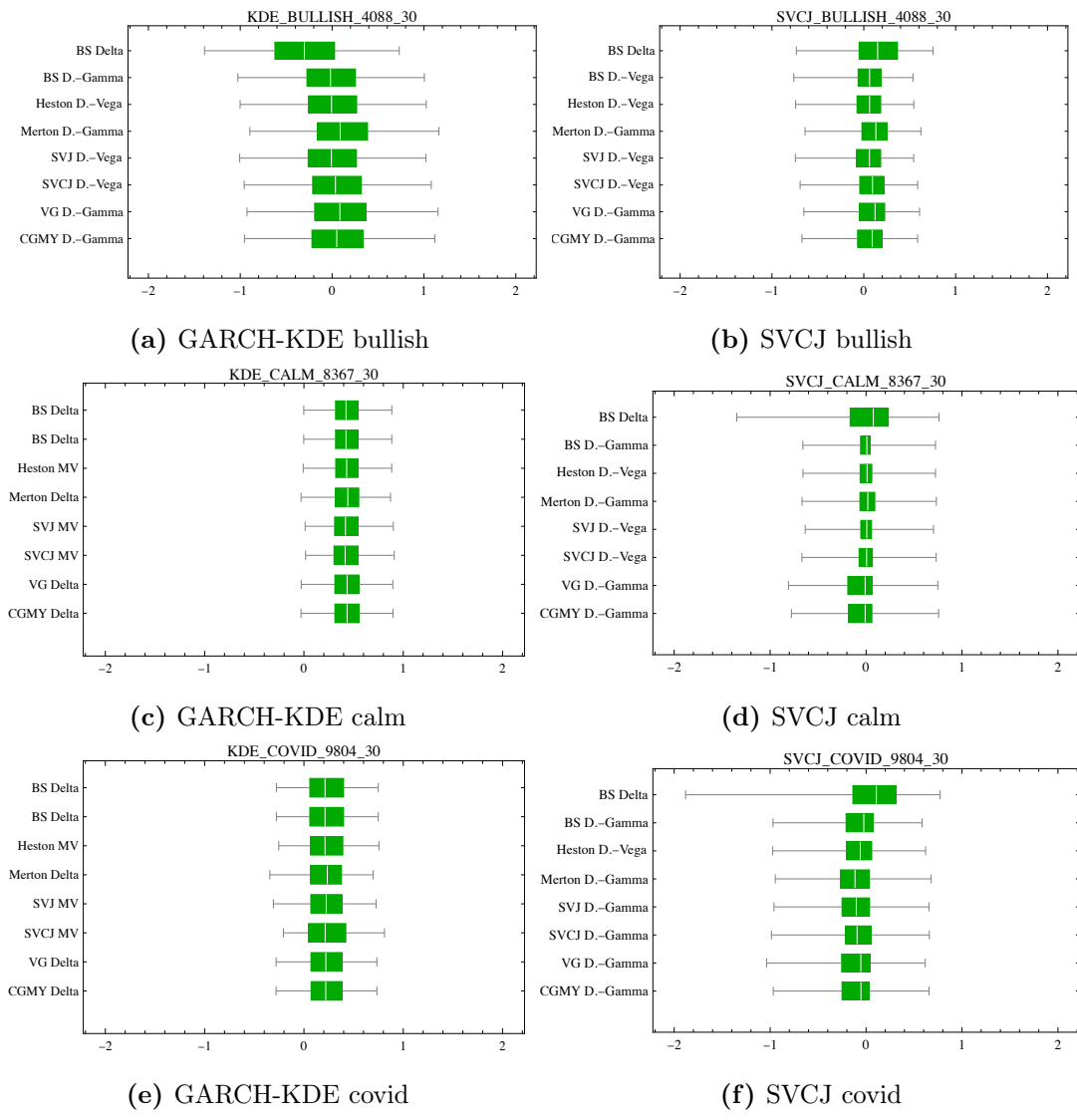
3.5 Hedge results

At the beginning of each market period, we short at-the-money options with maturities T = 1 M and T = 3 M at the option prices listed in Table 3.1. As outlined earlier, the price process is simulated in both SVCJ and the GARCH-KDE setting. The exposure in each option is dynamically hedged using the strategies summarized in Table 2.2. The hedge performance is evaluated in terms of π_{rel} with regard to the median q_{50}, hedge error ε_{rel}, tail measures $\mathrm{ES}_{5\%}$ and $\mathrm{ES}_{95\%}$ as well as extremes with results in Table 3.9 to Table 3.20. For a concise graphical representation, the best performing hedge strategies across models are compared in boxplots displayed in Figures 3.6 and Figures 3.7. For each model, the best performing strategy is selected according to $\mathrm{ES}_{5\%}$.

These are the main findings: First, with some exceptions, using multiple instruments for hedging, i.e., Delta-Gamma and Delta-Vega hedges, when compared to a simple Delta-hedge lead to a substantial reduction in tail risk. Hence, whenever liquidly traded options are available for hedging, they should be used. The calm and COVID periods in the GARCH-KDE approach are exceptions for the short-maturity option as well as the calm period and GARCH-KDE approach for the long-date option – here, no significant improvement is achieved by including a second hedge instrument. In the GARCH-KDE approach, paths are simulated from return residuals $\hat{Z}_t$. By definition, returns are correlated with S_t. Hence, under this market simulation, an important risk factor is the underlying itself. Especially on short time intervals, the option is most sensitive to the underlying itself. In any case, no deterioration takes place when using a second security for hedging.

Second, for short-dated options, no substantial differences occur in the optimal hedging strategies across models. The sole exception is worse performance of the VG- and CGMY-models in calm period when price paths are generated in the SVCJ model.

Third, turning to the long-dated option, although not always best performing, it can be said that stochastic volatility models perform *consistently* well. Amongst the stochastic volatility model, the SV model as the simplest model, does not underperform and sometimes even is the best-performing model. For the choice of a SV hedge model, the $\Delta_{SV} - \mathcal{V}_{SV}$ hedge is a replicating strategy (Kurpiel and Roncalli, 1999) and performs often better than other models under the same or different strategies. As calibrated jump intensities λ_{SVJ} and λ_{SVCJ} are low, the SVJ or SVCJ are often similar to the SV leading to comparable hedge results.

(a) GARCH-KDE bullish

(b) SVCJ bullish

(c) GARCH-KDE calm

(d) SVCJ calm

(e) GARCH-KDE covid

(f) SVCJ covid

Figure 3.6: Boxplot hedge performance comparison of π_{rel} for T = 1 M under (a) GARCH-KDE and (b) SVCJ market simulation. For illustrative purposes π_{rel} is truncated at $q_{5\%}$ and $q_{95\%}$. The vertical axis portrays Δ_{BS} hedge results compared to the best performing strategy of a given hedge model. The best performing strategy is selected for the minimal $ES_{5\%}$. 🔍hedging_cc

	Δ_{BS}	$\Delta-\Gamma_{BS}$	$\Delta-\mathcal{V}_{SV}$	$\Delta-\Gamma_{JD}$	$\Delta-\mathcal{V}_{SVJ}$	$\Delta-\mathcal{V}_{SVCJ}$	$\Delta-\Gamma_{VG}$	$\Delta-\Gamma_{CGMY}$
Min	**-3.35**	-2.58	-2.62	**-2.48**	-2.63	-2.59	-2.51	-2.53
$ES_{5\%}$	**-1.75**	-1.34	-1.32	**-1.21**	-1.32	-1.27	-1.24	-1.27
$ES_{95\%}$	**1.17**	1.49	1.51	**1.65**	1.5	1.57	1.64	1.61
Max	**3.31**	5.32	5.29	5.33	5.28	**5.35**	4.77	5.05
π_{rel}	**63.14**	59.55	59.39	60.43	**59.40**	59.75	60.97	60.87

Table 3.9: Hedge performance for T = 1 M under GARCH-KDE simulation in the *bullish* segment with the best and the worst in worst performing strategy.

	Δ_{BS}	$\Delta-\mathcal{V}_{BS}$	$\Delta-\mathcal{V}_{SV}$	$\Delta-\Gamma_{JD}$	$\Delta-\mathcal{V}_{SVJ}$	$\Delta-\mathcal{V}_{SVCJ}$	$\Delta-\Gamma_{VG}$	$\Delta-\Gamma_{CGMY}$
Min	**-11.35**	-9.46	-9.65	-9.69	-9.65	-9.58	-8.13	**-8.07**
$ES_{5\%}$	**-1.48**	-1.16	-1.16	**-1.06**	-1.16	-1.12	-1.08	-1.10
$ES_{95\%}$	1.02	**0.98**	**0.98**	1.11	**0.98**	1.04	**1.12**	1.10
Max	**18.69**	20.15	20.46	20.51	20.46	20.58	22.56	**24.47**
π_{rel}	**56.12**	50.7	50.2	51.36	**49.86**	50.37	52.32	52.56

Table 3.10: Hedge performance for T = 1 M under SVCJ simulation in the *bullish* segment with the best and the worst in worst performing strategy.

	Δ_{BS}	Δ_{BS}	MV_{SV}	Δ_{JD}	MV_{SVJ}	MV_{SVCJ}	Δ_{VG}	Δ_{CGMY}
Min	**-0.94**	**-0.94**	-1.01	-1.07	-1.03	-1.1	-1.16	**-1.18**
$ES_{5\%}$	-0.16	-0.16	-0.17	-0.19	**-0.15**	-0.15	**-0.2**	**-0.2**
$ES_{95\%}$	1.04	1.04	1.05	**1.03**	1.07	**1.09**	1.08	1.08
Max	**1.77**	**1.77**	1.81	1.8	**1.91**	1.86	1.8	1.81
π_{rel}	**25.44**	**25.44**	25.52	25.97	25.78	26.01	26.8	**26.87**

Table 3.11: Hedge performance for T = 1 M under GARCH-KDE *calm* with the best and worst performing strategy.

	Δ_{BS}	$\Delta-\Gamma_{BS}$	$\Delta-\mathcal{V}_{SV}$	$\Delta-\Gamma_{JD}$	$\Delta-\mathcal{V}_{SVJ}$	$\Delta-\mathcal{V}_{SVCJ}$	$\Delta-\Gamma_{VG}$	$\Delta-\Gamma_{CGMY}$
Min	**-8.07**	**-4.45**	**-4.45**	-5.07	**-4.45**	-4.46	-5.04	-6.24
$ES_{5\%}$	**-2.20**	-1.01	-1.00	-1.01	**-0.96**	-1.01	-1.19	-1.14
$ES_{95\%}$	1.13	1.12	1.12	1.13	**1.09**	1.13	1.15	**1.17**
Max	8.81	8.86	8.88	**12.07**	8.88	9.69	**8.73**	9.95
π_{rel}	**67.72**	43.78	43.66	44.58	**42.29**	44.34	48.69	48.24

Table 3.12: Hedge performance for T = 1 M under SVCJ *calm* segment with the best and worst performing strategy.

	Δ_{BS}	Δ_{BS}	MV_{SV}	Δ_{JD}	MV_{SVJ}	MV_{SVCJ}	Δ_{VG}	Δ_{CGMY}
Min	**-1.39**	**-1.39**	-1.28	-1.38	-1.29	**-1.23**	**-1.39**	**-1.39**
$ES_{5\%}$	-0.49	-0.49	-0.46	**-0.55**	-0.51	**-0.39**	-0.48	-0.48
$ES_{95\%}$	0.88	0.88	0.89	**0.83**	0.87	**0.96**	0.88	0.88
Max	1.37	1.37	1.39	**1.33**	1.38	**1.54**	1.44	1.43
π_{rel}	30.21	30.21	**29.52**	30.3	30.08	**30.78**	29.62	29.56

Table 3.13: Hedge performance for T = 1 M under GARCH-KDE *covid* with the best and worst performing strategy.

	Δ_{BS}	$\Delta-\Gamma_{BS}$	$\Delta-\mathcal{V}_{SV}$	$\Delta-\Gamma_{JD}$	$\Delta-\Gamma_{SVJ}$	$\Delta-\Gamma_{SVCJ}$	$\Delta-\Gamma_{VG}$	$\Delta-\Gamma_{CGMY}$
Min	-16.51	-10.93	**-10.88**	-14.36	-14.92	**-29.05**	-24.66	-17.07
ES$_{5\%}$	**-3.13**	**-1.64**	-1.72	-1.76	-1.76	-1.84	-1.85	-1.75
ES$_{95\%}$	1.08	**0.98**	1.01	1.09	1.08	**1.11**	1.00	1.06
Max	7.74	8.92	**7.00**	**21.48**	14.13	20.24	11.11	11.54
π_{rel}	**88.09**	**56.03**	57.62	60.19	60.53	63.85	61.3	58.33

Table 3.14: Hedge performance for T = 1 M under SVCJ *covid* with the **best** and **worst** performing strategy.

	Δ_{BS}	$\Delta-\Gamma_{BS}$	$\Delta-\mathcal{V}_{SV}$	$\Delta-\Gamma_{JD}$	$\Delta-\mathcal{V}_{SVJ}$	$\Delta-\mathcal{V}_{SVCJ}$	$\Delta-\Gamma_{VG}$	$\Delta-\Gamma_{CGMY}$
Min	**-6.55**	-6.36	-6.35	**-6.32**	-6.35	-6.34	-6.36	-6.37
ES$_{5\%}$	**-2.38**	-1.99	**-1.95**	-1.96	-1.97	**-1.95**	-1.98	-1.99
ES$_{95\%}$	**2.43**	2.83	2.8	**2.85**	2.81	2.81	2.83	2.83
Max	11.46	11.73	11.74	**11.76**	**11.00**	11.73	11.72	11.71
π_{rel}	**101.91**	101.76	**100.30**	101.77	101.02	100.72	101.75	101.75

Table 3.15: Hedge performance for T = 3 M GARCH-KDE *bullish* with the **best** and **worst** performing strategy.

	Δ_{BS}	$\Delta-\Gamma_{BS}$	$\Delta-\mathcal{V}_{SV}$	$\Delta-\Gamma_{JD}$	$\Delta-\mathcal{V}_{SVJ}$	$\Delta-\mathcal{V}_{SVCJ}$	$\Delta-\Gamma_{VG}$	$\Delta-\Gamma_{CGMY}$
Min	**-14.67**	-11.58	-11.57	-11.51	-11.55	**-9.30**	-11.6	-11.6
ES$_{5\%}$	**-1.10**	-0.64	-0.63	-0.62	-0.63	**-0.62**	-0.63	-0.63
ES$_{95\%}$	**0.84**	0.64	0.62	0.66	**0.62**	0.64	0.65	0.65
Max	10.14	**11.42**	11.29	11.34	11.26	**9.02**	11.27	11.27
Hedge error	**44.14**	26.5	25.86	26.45	25.89	**25.26**	26.55	26.39

**Table 3.16:** Hedge performance for T = 3 M SVCJ *bullish* with the **best** and **worst** performing strategy.

	Δ_{BS}	Δ_{BS}	MV$_{SV}$	Δ_{JD}	MV$_{SVJ}$	Δ_{SVCJ}	Δ_{VG}	Δ_{CGMY}
Min	**-0.29**	**-0.29**	-0.27	-0.28	**-0.25**	**-0.25**	-0.28	-0.28
ES$_{5\%}$	0.18	0.18	**0.20**	**0.15**	0.19	**0.20**	0.19	0.19
ES$_{95\%}$	0.76	0.76	0.76	**0.73**	**0.77**	0.75	0.75	0.75
Max	**1.04**	**1.04**	1.06	1.05	**1.12**	1.07	1.12	1.12
π_{rel}	13.59	13.59	13.11	13.53	**13.82**	**12.82**	13.18	13.18

Table 3.17: Hedge performance for T = 3 M GARCH-KDE *calm* with the **best** and **worst** performing strategy.

	Δ_{BS}	$\Delta-\Gamma_{BS}$	$\Delta-\mathcal{V}_{SV}$	$\Delta-\mathcal{V}_{JD}$	$\Delta-\mathcal{V}_{SVJ}$	$\Delta-\mathcal{V}_{SVCJ}$	$\Delta-\Gamma_{VG}$	$\Delta-\Gamma_{CGMY}$
Min	-12.63	-8.68	**-12.75**	**-6.32**	-7.79	-12.75	-12.73	-12.74
ES$_{5\%}$	**-1.56**	-0.85	**-0.71**	-0.79	-0.78	-0.89	-0.96	-0.97
ES$_{95\%}$	0.88	0.82	**0.69**	0.77	0.79	0.88	0.89	**0.90**
Max	7.74	5.19	7.79	**4.15**	7.78	8.99	8.97	**9.25**
Hedge error	**53.39**	33.36	**28.28**	31.01	31.26	36.05	38.82	39.09

Table 3.18: Hedge performance for T = 3 M SVCJ *calm* with the **best** and **worst** performing strategy.
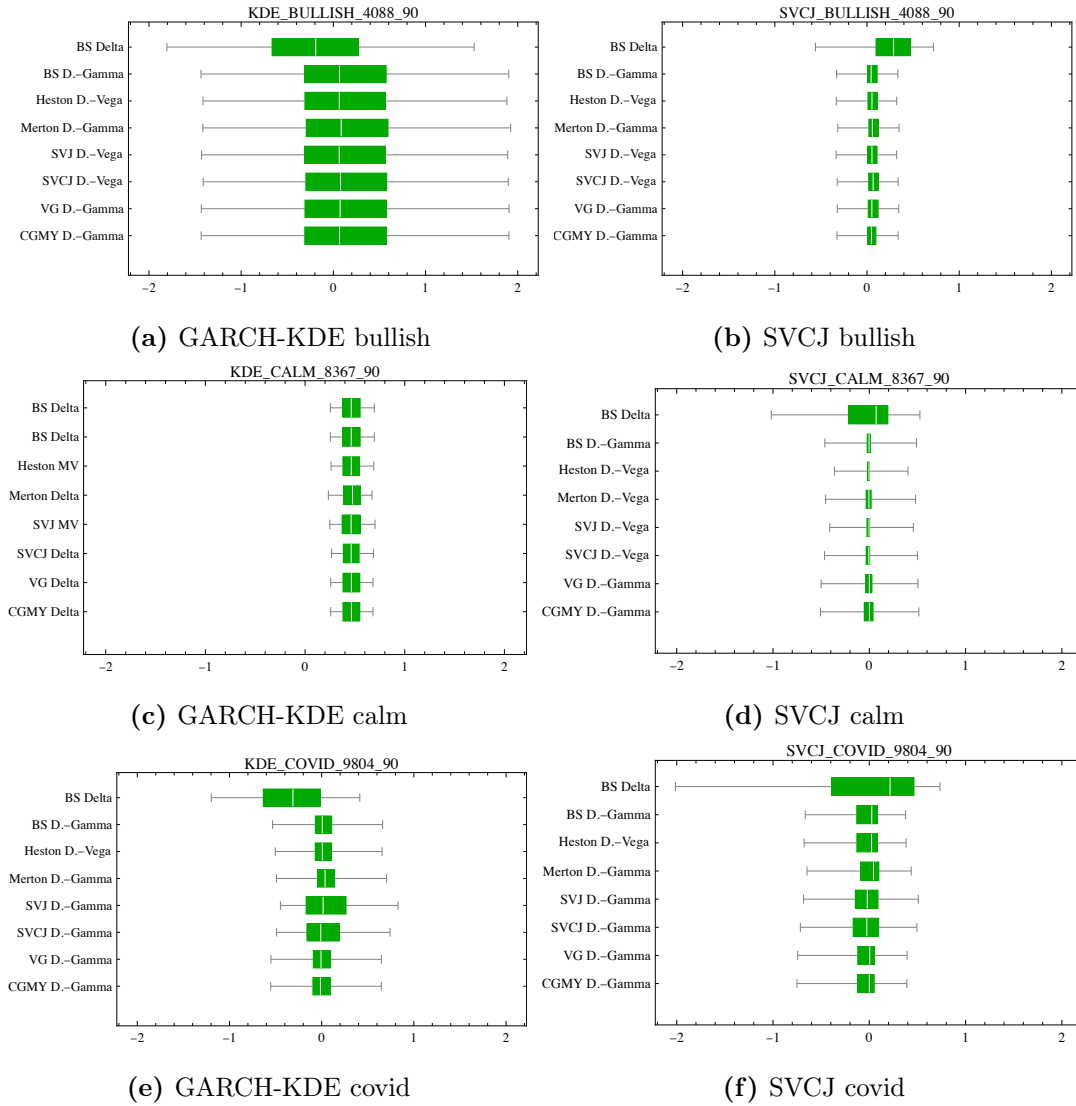
Figure 3.7: Boxplot hedge performance comparison of π_{rel} for T = 3 M under (a) GARCH-KDE and (b) SVCJ market simulation. For illustrative purposes π_{rel} is truncated at $q_{5\%}$ and $q_{95\%}$. The vertical axis portrays Δ_{BS} hedge results compared to the best performing strategy of a given hedge model. The best performing strategy is selected for the minimal $ES_{5\%}$.

	Δ_{BS}	$\Delta-\Gamma_{BS}$	$\Delta-\mathcal{V}_{SV}$	$\Delta-\Gamma_{JD}$	$\Delta-\Gamma_{SVJ}$	$\Delta-\Gamma_{SVCJ}$	$\Delta-\Gamma_{VG}$	$\Delta-\Gamma_{CGMY}$
Min	**-4.36**	-2.69	-2.64	-2.64	**-2.44**	-2.58	-2.7	-2.71
$ES_{5\%}$	**-1.56**	-0.8	-0.76	-0.77	**-0.70**	-0.78	-0.83	-0.84
$ES_{95\%}$	**0.6**	0.93	0.9	0.97	**1.11**	1.00	0.91	0.9
Max	3.88	3.33	**3.32**	4.52	**4.57**	4.45	4.49	4.55
π_{rel}	**50.06**	34.48	**33.09**	34.57	40.02	37.4	34.63	34.67

Table 3.19: Hedge performance for T = 3 M GARCH-KDE *covid* with the **best** and **worst** performing strategy.

	Δ_{BS}	$\Delta-\Gamma_{BS}$	$\Delta-\mathcal{V}_{SV}$	$\Delta-\Gamma_{JD}$	$\Delta-\Gamma_{SVJ}$	$\Delta-\Gamma_{SVCJ}$	$\Delta-\Gamma_{VG}$	$\Delta-\Gamma_{CGMY}$
Min	-13.53	**-7.89**	-7.9	-14.3	-11.76	-11.75	**-20.99**	-11.72
$ES_{5\%}$	**-2.77**	**-1.18**	-1.26	-1.34	-1.36	-1.39	-1.26	-1.25
$ES_{95\%}$	0.87	0.71	**0.68**	0.78	**0.94**	0.93	0.73	0.73
Max	13.48	10.78	**10.77**	13.60	13.66	13.6	**13.67**	13.65
Hedge error	**88.42**	**38.24**	39.34	43.95	48.	49.06	42.99	41.27

Table 3.20: Hedge performance for T = 3 M SVCJ *covid* with the **best** and **worst** performing strategy.

25

4   Conclusion

We provide hedge results for hedging CC options in diverse market behavior segments under different market generation approaches. First, multiple-instrument hedging strategies lead to considerable PnL volatility and tail risk reduction. As short-dated options are less sensitive to volatility or higher-order sensitivities, differences across strategies and model choice are less pronounced. For longer-dated options, persistently good hedge results are achieved for hedging with stochastic volatility models. Returns are mainly driven by stochastic volatility with infrequent jumps, which cannot be hedged anyway.

.1 Hedge routine

We illustrate the dynamic hedging routing on a single instrument self-financed hedging strategy ξ and apply it analogously for all other hedging strategies considered in this study. At time $t = 0$ and for $B(0) = B_{0,i} = 1$ the value of the portfolio for the self-financed strategy ξ is

$$V(0) = C(0, S(0)) = \xi(0)S(0) + \{C(0, S(0)) - \xi(0)S(0)\} B(0)$$
$$M(0) = C(0, S(0)) - \xi(0)S(0) \tag{18}$$

where $B(t)$ is a risk-free asset and $M(t)$ the money market account vector. The value of the portfolio at time $t > 0$ is

$$M(t) = M(t - dt) + \{\xi(t - dt) - \xi(t)\} \frac{S(t)}{B(t)}$$
$$V(t) = \xi(t - dt)S(t) + M(t - dt)B(t - dt)e^{rdt} = \xi(t)S(t) + \underbrace{\frac{V(t) - \xi(t)S(t)}{B(t)}}_{=M(t)} B(t) \tag{19}$$

At maturity T, the final PnL distribution vector is

$$V(T) = \xi(T - dt)S(t) + M(T - dt)B(t) \tag{20}$$

.2 Dynamic Delta-hedging

The option writer shorts the call $C(t)$, longs the underlying $S(t)$ and sends the remainder to a money market account $B(t)$ for which

$$dB(t) = rB(t)dt$$

At time t, the value of portfolio $V(t)$ is

$$V(t) = -C(t) + \Delta(t)S(t) + \frac{\{C(t) - \Delta(t)S(t)\}}{B(t)}B(t) \tag{21}$$

The changes evolve through

$$dV(t) = -dC(t) + \Delta(t)dS(t) + \{C(t) - \Delta(t)S(t)\} rdt \tag{22}$$

.3 Dynamic Delta-Gamma-hedging

We will explain the $\Delta - \mathcal{V}$ hedge in detail. The $\Delta - \Gamma$- hedge is performed accordingly. This strategy eliminates the sensitivity to changes in the underlying and changes in volatility.

The option writer shorts the call option C, takes the position Δ in the asset and Λ in the second contingent claim. At time t, the value of the portfolio is

$$V(t) = -C(t) + \Lambda C_1(t) + \Delta S(t) \tag{23}$$

with the change in the portfolio $V(t)$

$$dV(t) = \Delta(t)dS + \{C(t) - \Delta S(t) - \Lambda C_2(t)\}\, rdt - dC(t) + \Lambda dC_2(t) \tag{24}$$

That is

$$
\begin{aligned}
dV(t) = {}& (C(S,V,t) - \Delta S(t) - \Lambda C_2(S,V,t))\, rdt \\
& - \left(\frac{\partial C}{\partial t} + \frac{1}{2}\frac{\partial^2 C}{\partial S^2}VS^2 + \frac{1}{2}\frac{\partial^2 C}{\partial V^2}^2 V + \frac{\partial^2 C}{\partial V \partial S}\rho V S \right) dt \\
& + \Lambda \left(\frac{\partial C_2}{\partial t} + \frac{1}{2}\frac{\partial^2 C_2}{\partial S^2}VS^2 + \frac{1}{2}\frac{\partial^2 C_2}{\partial V^2}^2 V + \frac{\partial^2 C_2}{\partial V \partial S}\rho V S \right) dt \\
& + \left(\Lambda \frac{\partial C_2}{\partial S} - \frac{\partial C}{\partial S} + \Delta \right) dS + \left(\Lambda \frac{\partial C_2}{\partial V} - \frac{\partial C}{\partial V} \right) dV
\end{aligned}
\tag{25}
$$

For the choice of

$$\Delta = \frac{\partial C}{\partial S} - \Lambda \frac{\partial C_2}{\partial S}$$

$$\Lambda = \frac{\partial C/\partial v}{\partial C_2/\partial v}$$

the portfolio is $\Delta - \mathcal{V}$ hedged. Analogously, for the choice of

$$\Delta = \frac{\partial C}{\partial S} - \Lambda \frac{\partial C_2}{\partial S}$$

$$\Lambda = \frac{\partial^2 C}{\partial^2 S}$$

this is a $\Delta - \Gamma$ hedge. For comparison, these hedges are applied to all models in the class of affine jump diffusion models.

.4   Alternative representation of the VG process

The alternative representation of the **VG** process has the characteristic function

$$\varphi_{\mathrm{VG}}(u; C, G, M) = \left(\frac{GM}{GM + (M - G)\mathrm{i}u + u^2} \right)^C \tag{26}$$

where $C, G, M > 0$ with

$$C = 1/\nu$$

$$G = \left(\sqrt{\frac{1}{4}\theta^2\nu^2 + \frac{1}{2}\sigma^2\nu} - \frac{1}{2}\theta\nu \right)^{-1} \tag{27}$$

$$M = \left(\sqrt{\frac{1}{4}\theta^2 v^2 + \frac{1}{2}\sigma^2\nu} + \frac{1}{2}\theta\nu \right)^{-1}$$

28

An increase in G increases the size of upward jumps, while an increase in M increases the size of downward jumps. Accordingly, θ, M and G account for the skewness of the distribution. C governs the Levy-measure by widening it with its increase and narrowing it with its decrease.

.5 Tables

TTM	a	b	ρ	m	σ	penalty
0.01	0.17	0.10	0.00	0.00	1.00	24.53
0.03	0.003	0.01	0.15	0.01	0.17	0.00001
0.07	0.01	0.04	0.00	-0.01	0.08	0.000004
0.24	0.02	0.10	-0.11	-0.01	0.45	0.001
0.49	0.01	0.17	-0.02	0.04	0.77	0.002
0.74	0.14	0.09	0.00	0.01	0.93	0.03
0.01	0.001	0.05	-0.13	0.02	0.08	0.09
0.03	0.01	0.05	-0.39	0.01	0.16	0.01
0.07	0.01	0.10	-0.02	0.12	0.32	0.02
0.16	0.06	0.15	-0.50	-0.17	0.54	0.01
0.24	0.04	0.19	-0.27	-0.10	0.76	0.03
0.49	0.18	0.21	0.23	0.38	1.00	0.01
0.02	0.004	0.02	0.50	0.02	0.01	0.03
0.04	0.003	0.05	-0.07	-0.03	0.11	0.01
0.07	0.01	0.08	-0.09	-0.05	0.15	0.02
0.15	0.02	0.13	0.19	0.07	0.29	0.04
0.40	0.06	0.20	-0.15	-0.21	0.56	0.01
0.65	0.14	0.18	0.16	-0.12	0.88	0.02

Table .1: Calibrated SVI parameters at the beginning of the bullish, calm and stressed segment. hedging_cc

	SV	SVJ	SVCJ
$\hat{\mu}$	0.82	0.78	0.87
$\hat{\sigma}$	0.32	0.33	0.35
min	0.00	0.00	0.00
q_{25}	0.62	0.62	0.69
q_{50}	0.84	0.81	0.92
q_{75}	1.04	0.99	1.06
max	1.49	1.57	2.43
$\hat{\mu}$	0.68	0.72	0.90
$\hat{\sigma}$	0.30	0.36	0.37
min	0.00	0.00	0.00
q_{25}	0.50	0.56	0.70
q_{50}	0.75	0.79	1.02
q_{75}	0.90	0.95	1.19
max	1.43	1.40	1.44
$\hat{\mu}$	0.56	0.72	0.84
$\hat{\sigma}$	0.49	0.66	0.45
min	0.00	0.00	0.00
q_{25}	0.27	0.29	0.61
q_{50}	0.50	0.73	0.88
q_{75}	0.78	1.01	1.04
max	3.83	6.33	3.83

Table .2: Summary statistics of σ_v for all 3 market segments and models.

 hedging_cc

.6 Additional plots
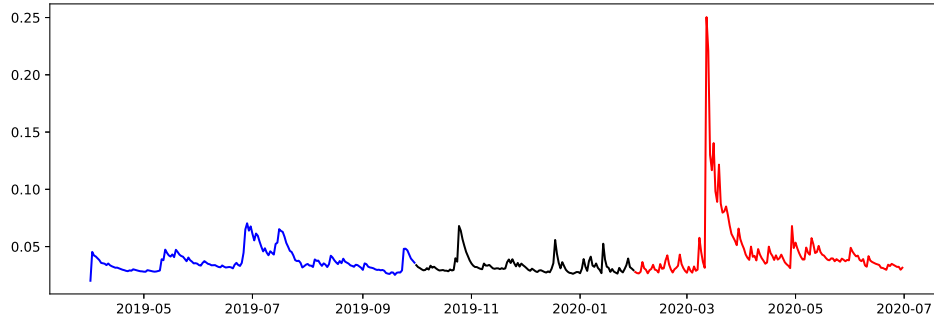
Figure .1: Estimated GARCH(1,1) volatility $\hat{\sigma}_t$ during bullish market behavior, calm period and stressed scenario. hedging_cc
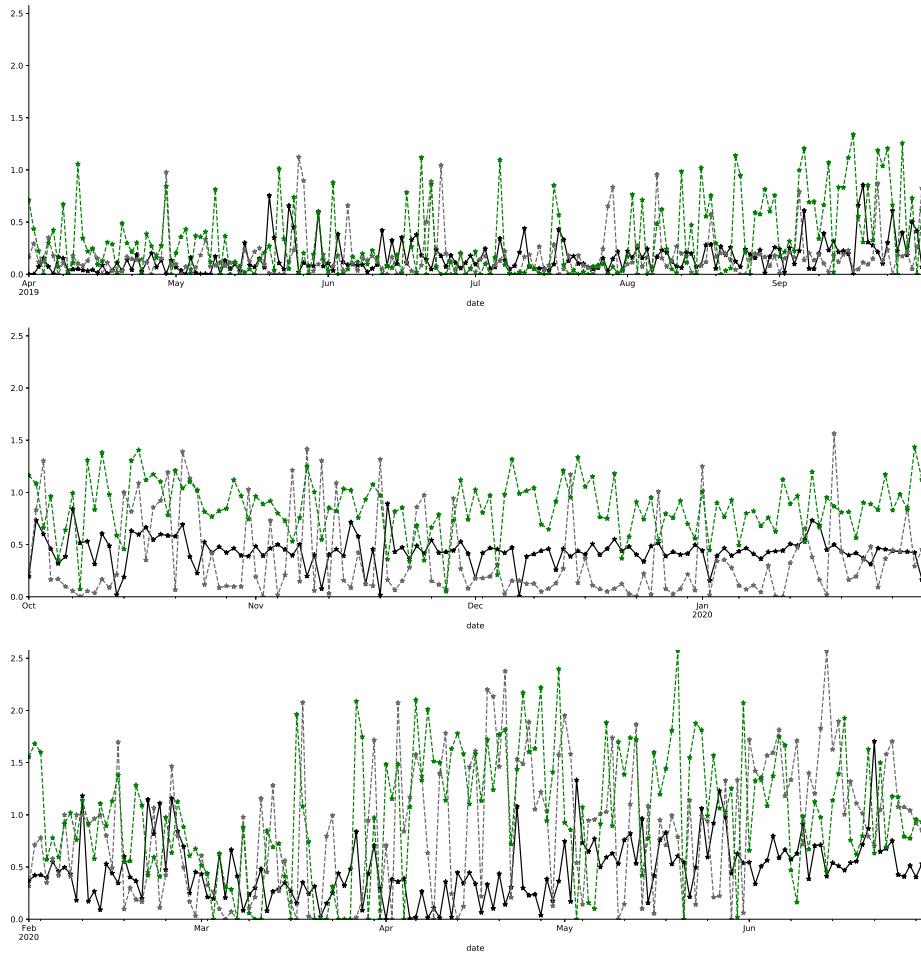
Figure .2: Daily calibrated jump intensity λ_{JD}, λ_{SVJ} and λ_{SVCJ} segregated chronologically by market segment. In all market segments, yearly jump intensity is generally $\lambda \leq 2$.
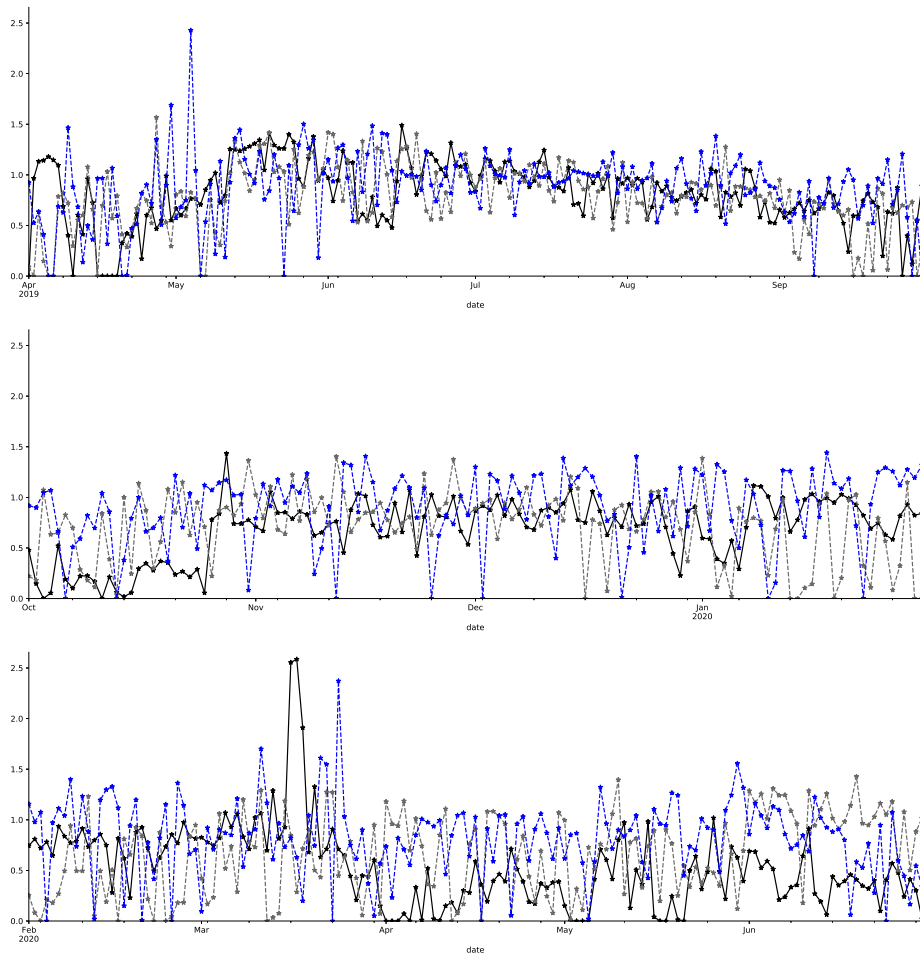
Figure .3: Daily calibrated volatility of volatility $\sigma_{v_{SV}}$, $\sigma_{v_{SVJ}}$ and $\sigma_{v_{SVCJ}}$ plotted in chronological order by market segment. For illustrative purposes, extremes are disregarded. Information on extremes is provided in Table .2. Regardless of the model choice, levels of σ_v are high. This provides strong indication for stochastic volatility.
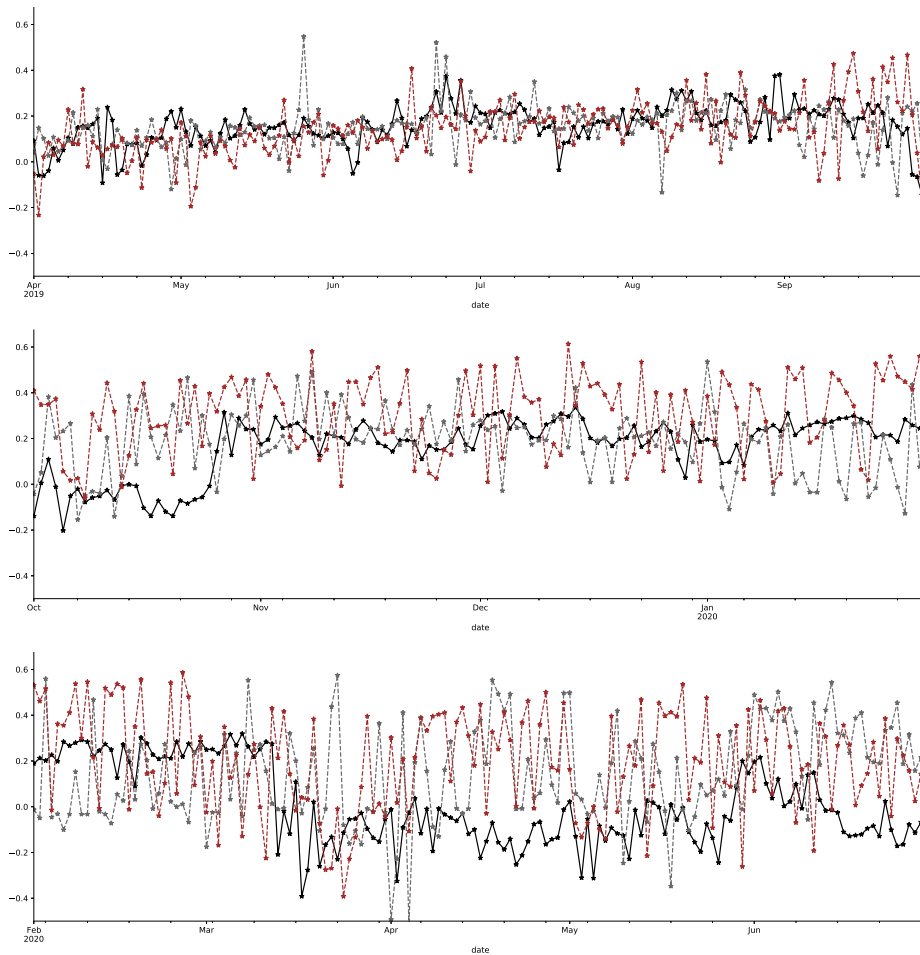
Figure .4: Daily calibrated correlation parameter ρ_{SV}, ρ_{SVJ} and ρ_{SVCJ} plotted in chronological order by market segment. For illustrative purposes, extremes are disregarded. As generally $\rho > 0$, there is a strong indication for an inverse leverage effect.
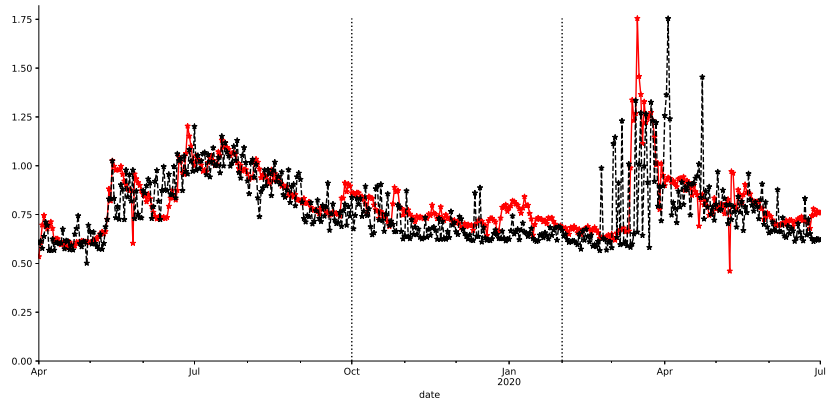
Figure .5: Daily calibration of σ_{VG} plotted against σ_{BS}. Both models capture comparable volatility levels.
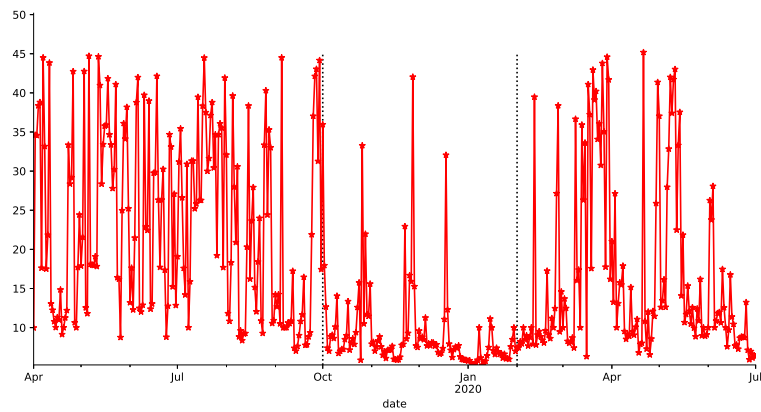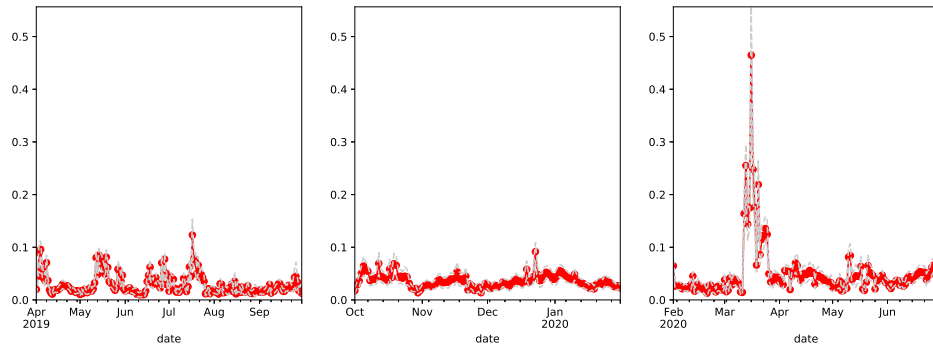
(a) downward jumps M
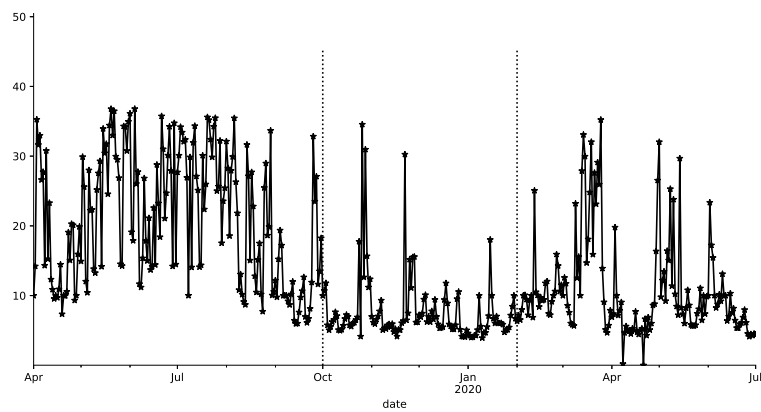
(b) upward jumps G

Figure .6: (a) Evolution of G_{CGMY} and (b) M_{CGMY} segregated by market segment. High magnitudes for both parameter values are observed during the *bullish* and *stressed* scenario. For illustrative purposes, extremes are excluded from this graph.
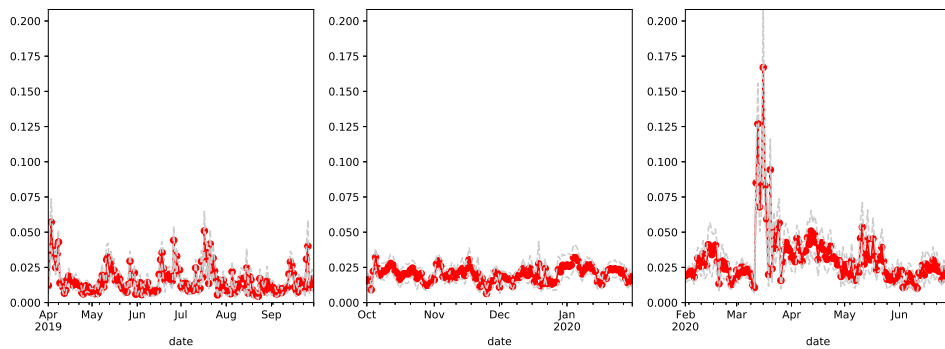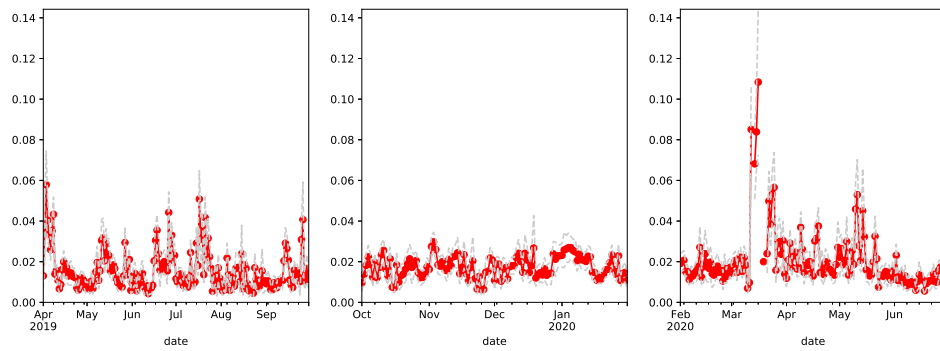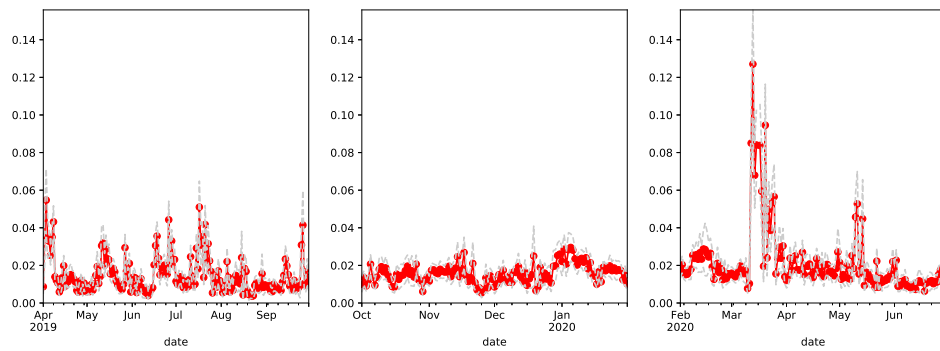
36
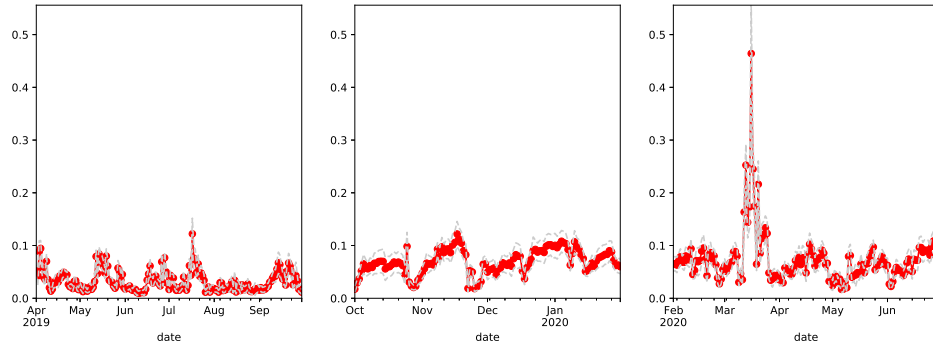
.7 RMSE

(a) BS

(b) JD

(c) SV

Figure .7: RMSE with 95 %-confidence band of the (a) BS, (b) JD and (c) SV model.
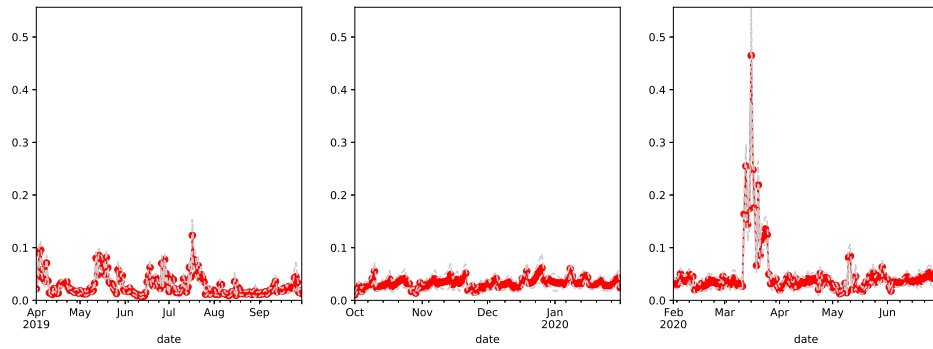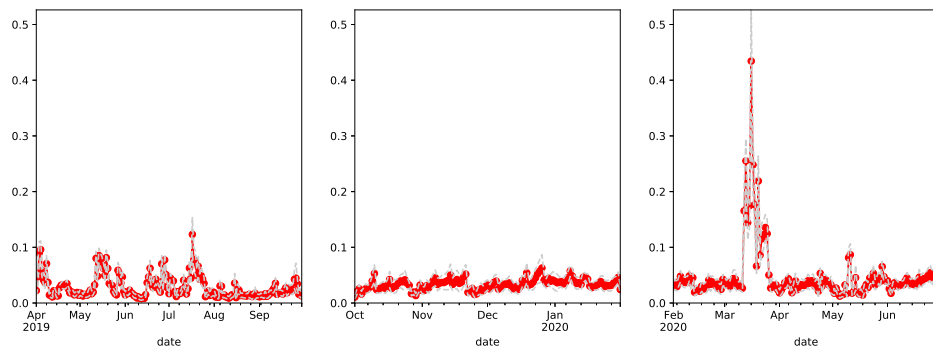
(a) SVJ

(b) SVCJ

Figure .8: RMSE with 95 %-confidence band of the (a) SVJ, (b) SVCJ, (c) VG and (d) CGMY model.

(a) VG

(b) CGMY

Figure .9: RMSE with 95 %-confidence band of the (a) VG and (b) CGMY model.

References

David S Bates. Jumps and stochastic volatility: Exchange rate processes implicit in deutsche mark options. *The Review of Financial Studies*, 9(1):69–107, 1996.

Anatoliy Belaygorod. Solving continuous time affine jump-diffusion models for econometric inference. *John M. Olin School of Business working paper*, 12 2005.

Fischer Black and Myron Scholes. The pricing of options and corporate liabilities. *Journal of Political Economy*, 81(3):637–54, 1973.

Tim Bollerslev. Generalized autoregressive conditional heteroskedasticity. *Journal of Econometrics*, 31(3):307 – 327, 1986.

Nicole Branger, Alexandra Hansis, and Christian Schlag. Expected option returns and the structure of jump risk premia. *EFA 2009 Bergen Meetings Paper*, 02 2009.

Nicole Branger, Eva Krautheim, Christian Schlag, and Norman Seeger. Hedging under model misspecification: All risk factors are equal, but some are more equal than others . . . . *Journal of Futures Markets*, 32:397 – 430, 05 2012. doi: 10.1002/fut.20530.

Mark Broadie, Mikhail Chernov, and Michael Johannes. Model specification and risk premia: Evidence from futures options. *The Journal of Finance*, 62(3):1453–1490, 2007.

Peter Carr and Helyette Geman. The fine structure of asset returns: An empirical investigation. *The Journal of Business*, 75(2):305–332, 2002.

Peter Carr and Dilip Madan. Option valuation using the fast fourier transform. *Journal of Computational Finance*, 2, 03 2001. doi: 10.21314/JCF.1999.043.

Mikhail Chernov, A. Gallant, Eric Ghysels, and George Tauchen. Alternative models for stock price dynamics. *Journal of Econometrics*, 116(1-2):225–257, 2003.

Nils Detering and Natalie Packham. Model risk in incomplete markets with jumps. *Springer Proceedings in Mathematics and Statistics*, 99:39–59, 01 2015. doi: 10.1007/ 978-3-319-09114-3_3.

Darrell Duffie, Jun Pan, and Kenneth Singleton. Transform analysis and asset pricing for affine jump diffusions. *Econometrica*, 68(6):1343–1376, 2000.

Bjørn Eraker. Do stock prices and volatility jump? reconciling evidence from spot and option prices. *The Journal of Finance*, 59(3):1367–1403, 2004.

Bjørn Eraker, Michael Johannes, and Nicholas Polson. The impact of jumps in volatility and returns. *The Journal of Finance*, 58(3):1269–1300, 2003.

H. Föllmer and D. Sondermann. Hedging of non-redundant contingent claims. 1985.

Jim Gatheral. A parsimonious arbitrage-free implied volatility parameterization with application to the valuation of volatility derivatives. *Presentation at Global Derivatives & Risk Management, Madrid*, 2004.

Jim Gatheral and Antoine Jacquier. Arbitrage-free svi volatility surfaces. *Quantitative Finance*, 14(1):59–71, 2014.

Steven L Heston. A closed-form solution for options with stochastic volatility with applications to bond and currency options. *The review of financial studies*, 6(2):327–343, 1993.

AJ Hou, Weining Wang, K Chen, and Wolfgang Karl CYH, Härdle. Pricing cryptocurrency options: the case of crix and bitcoin. *Journal of Financial Econometrics*, 2020. doi: 10.1007/s42521-019-00002-1.

Wolfgang Karl Härdle and Simon Trimborn. Crix or evaluating blockchain based currencies. *The Mathematics and Statistics of Quantitative Risk Management - Oberwolfach Reports*, 2015(42):2497 – 2500, 2015.

Alisa Kim, Simon Trimborn, and Wolfgang Karl Härdle. Vcrix — a volatility index for crypto-currencies. *International Review of Financial Analysis*, page 101915, 2021. doi: https://doi.org/10.1016/j.irfa.2021.101915.

D. Kraft. *A software package for sequential quadratic programming.* Deutsche Forschungs- und Versuchsanstalt für Luft- und Raumfahrt Köln: Forschungsbericht. Wiss. Berichtswesen d. DFVLR, 1988.

Adam Kurpiel and Thierry Roncalli. Option hedging with stochastic volatility. 01 1999. doi: 10.2139/ssrn.1031927.

Dilip B. Madan, Peter P. Carr, and Eric C. Chang. The variance gamma process and option pricing. *Review of Finance*, 2(1):79–105, 1998.

Dilip B. Madan, Sofie Reyners, and Wim Schoutens. Advanced model calibration on bitcoin options. *Digital Finance*, 1(1):117–137, 2019. doi: 10.1007/s42521-019-00002-1.

Alexander J. McNeil and Rudiger Frey. Estimation of tail-related risk measures for heteroscedastic financial time series: an extreme value approach. *Journal of Empirical Finance*, 7(3-4):271–300, 2000.

Robert C Merton. Option pricing when underlying stock returns are discontinuous. *Journal of financial economics*, 3(1-2):125–144, 1976.

Rolf Poulsen, Klaus Schenk-Hoppé, and Christian-Oliver Ewald. Risk minimization in stochastic volatility models: model risk and empirical performance. *Quantitative Finance*, 9(6):693–704, 2009.

Philip E. Protter. *Stochastic Integration and Differential Equations.* Stochastic Modelling and Applied Probability. Springer Berlin Heidelberg, 2005.

Olivier Scaillet, Adrien Treccani, and Christopher Trevisan. High-frequency jump analysis of the bitcoin market*. *Journal of Financial Econometrics*, 18(2):209–232, 06 2018. doi: 10.1093/jjfinec/nby013.

A.N. Tikhonov, A.S. Leonov, and A.G. Yagola. *Nonlinear ill-posed problems.* De Gruyter, 2011. doi: doi:10.1515/9783110883237.505.

Simon Trimborn and Wolfgang Karl Härdle. Crix an index for cryptocurrencies. *Journal of Empirical Finance*, 49:107–122, 12 2018.